CD82 Protects Against Glaucomatous Axonal Transport Deficits via mTORC1 Activation in Mice

Yin Zhao
Tongji Hospital, Tongji Medical College, Huazhong University of Science and Technology
https://orcid.org/0000-0002-1470-7184
Meng Ye
Tongji Hospital of Tongji Medical College of Huazhong University of Science and Technology
Jingqiu Huang
Tongji Hospital of Tongji Medical College of Huazhong University of Science and Technology
Qianxue Mou
Tongji Hospital of Tongji Medical College of Huazhong University of Science and Technology
Jing Luo
Huazhong University of Science and Technology
Yuanyuan Hu
Tongji Hospital of Tongji Medical College of Huazhong University of Science and Technology
Xiaotong Lou
Tongji Hospital of Tongji Medical College of Huazhong University of Science and Technology
Ke Yao
Tongji Hospital of Tongji Medical College of Huazhong University of Science and Technology
Bowen Zhao
Tongji Hospital of Tongji Medical College of Huazhong University of Science and Technology
Qiming Duan
Gladstone Institute of Cardiovascular Disease
Xing Li
Tongji Hospital of Tongji Medical College of Huazhong University of Science and Technology
Hong Zhang (tjyksys@163.com)
Tongji Hospital of Tongji Medical College of Huazhong University of Science and Technology

Research article

Keywords: Glaucoma, progressive optic nerve degeneration, retinal ganglion cell, optic nerve

Posted Date: April 14th, 2021

DOI: https://doi.org/10.21203/rs.3.rs-404388/v1

Abstract

Background:

Glaucoma is a leading cause of irreversible blindness worldwide characterized by progressive optic nerve degeneration and retinal ganglion cell (RGC) loss. Axonal transport deficits have been demonstrated to be the earliest crucial pathophysiological changes underlying axonal degeneration in glaucoma. The critical feature of this pathological process and the significance of early intervention remain to be further explored. Here, we explore the role of a tetraspanin superfamily member CD82 in protection of glaucomatous neurodegeneration in an acute ocular hypertension mouse model.

Methods:

Expression level of CD82 in retina was examined before and after an acute ocular hypertension (AOHT) model in mouse. Overexpression of CD82 was achieved by intraocular injection of adeno-associated virus vector expressing CD82. Axonal transport deficits were evaluated by intravitreally injected Cholera toxin B (CTB) from eyes to superior colliculus and the distribution of endogenous synaptophysin. Subsequent optic nerve (ON) degeneration phenotypes were also examined including axon loss, myelin damage, and Aβ accumulation. In vitro neurite outgrowth assay was performed in SH-SY5Y cells with Cd82-plasmid transfection. Another optic nerve crush (ONC) model was taken to further validate the neuroprotective effects of CD82 by evaluation of axonal regeneration, RGC survival, and visual function of mice. Downstream pathway of CD82 was analyzed by qPCR examination and western blotting analysis as well as phenotype detection.

Results:

We found a transient downregulation of CD82 after acute IOP elevation, with parallel emergence of axonal transport deficits. Overexpression of CD82 with AAV2/9 vector in mouse retina improved optic nerve (ON) axonal transport and ameliorated subsequent axon degeneration. In vitro neurite outgrowth assay displayed longer neurite length of SH-SY5Y cells with transfection of Cd82-plasmid. Moreover, CD82 overexpression could stimulate ON regeneration and restore mouse vision after an optic nerve crush model. CD82 exerted protective effect through upregulation of TRAF2, which was an E3 ubiquitin ligase and activated mTORC1 through K63-linked ubiquitylation and intracellular repositioning of Raptor.

Conclusions:

These findings indicate that CD82 overexpression protects against glaucomatous axonal transport deficits through TRAF2-dependent activation of mTORC1 pathway, which offers deeper insights into tetraspanins superfamily and demonstrated potential neuroprotective strategy in glaucoma treatments.

Background

Glaucoma is a neurodegenerative disease characterized by progressive loss of retinal ganglion cells (RGCs) and visual field(1). Increased intraocular pressure (IOP) is one of the most important risk factors of glaucoma. Though RGC apoptosis was doubtlessly critical in disease development, new insight of glaucoma nowadays trended to deemphasize RGC death, which was known to appear late in course, and pay more attention to the early axonal lesions(1). Axonal transport is important in maintaining proper neuronal function in visual pathway, since the RGC is highly polarized and has a long axon. Axon transport impairments have been identified as the earliest crucial pathophysiological changes underlying axonal degeneration in glaucoma(3), as well as other neurodegenerative diseases, such as Huntington's disease(4), amyotrophic lateral sclerosis(4), Parkinson's disease(6) and Alzheimer's disease(7). To explain how increased IOP contributes to axon damage, it is proposed that in eyes with raised IOP, the pressure difference across the optic nerve head (ONH) increases, compressing optic nerve, thus impedes antero- and retrograde axonal transport(8, 9). However, the critical feature of this process and the significance of early intervention remain to be further explored.

CD82 is a membrane glycoprotein belonging to the transmembrane 4 superfamily, also known as the tetraspanin superfamily. The tetraspanin family is evolutionarily-conserved, regulating immune systems, tumors, and cell proliferation(10). A number of tetraspanins also play critical roles in neuronal signaling and retinal degeneration(10). Tetraspanin 7 promoted glutamatergic synapses maturation as well as axonal branching during development(12, 13). Mutations in the peripherin/ RDS tetraspanin alone, or synergized with mutations in the ROM1 tetraspanin, disrupted the structure of outer segments of photoreceptor cells, resulting in retinal degeneration(14). CD82 is ubiquitously expressed in human tissues and well-known as a tumor suppressor protein(15), its effects in neuronal system, specifically in retina, has not been characterized yet.

The mechanistic target of rapamycin (mTOR) signaling pathway plays a vital role in cell growth, metabolism, as well as neuronal function(16). Dysregulation of mTOR pathway is involved in neurodegenerative diseases such as Alzheimer disease, Parkinson disease and in addition, glaucoma(16). In DBA/2J mice, an axon-protective ketogenic diet activated mTOR pathway, implying a potential role of mTOR pathway in maintaining proper structure and function of RGCs(18). A proteomic analysis of retina samples from ocular hypertension pateints and normotensive controls also revealed significant proteomic alterations in mTOR pathway(19). Moreover, Brain-derived neurotrophic factor (BDNF), a well-characterized neurotrophic factor in brain, activated mTOR complex 1 (mTORC1) and its downstream target phospho-S6 ribosomal protein kinase (pS6K)(20). Immunoprecipitation studies have revealed the expression of mTOR components in the inner retina with mTORC1 predominantly localized in RGCs and their axons, thus directly involved in regulating RGC axonal function, and mTORC2 primarily in glial cells to maintain homeostatic environment of the RGCs(21).

Proteins of the mTOR pathway are also capable to interact with a subset of tetraspanins. For example, tetraspanin 8 interacted with rictor, a key component of mTOR complex 2 (mTORC2) in malignant glioma(22). CD9 (TSPAN29) induced senescence in human endothelial cells via regulating PI3K/AKT-mTOR pathway(23). It is also reported that CD82 overexpression in multiple

myeloma cell lines resulted in upregulation of phospho-S6 ribosomal protein, an established target of mTORC1(24). However the specific mechanism underlying such regulation still remains unclear.

TRAF2 was a pivotal member of tumor necrosis factor (TNF) receptor associated factors (TRAFs) family, with an E3 ubiquitin ligase activity and possessing the ability to regulate multiple downstream signaling pathways via catalyzing linkages of polyubiquitin chains to specific substrates(24). For instance, K48-linked chains generally targeted substrates for proteasomal degradation, while K63-linked ubiquitination mostly mediated signal activation with a broader range of biological functions(28, 29). It has been reported that K63-linked ubiquitination was involved in regulating mTORC1 activity through ubiquitin modification of different components and recruiting them to the lysosome for further activation(30-32).

In the present study, we investigated roles of CD82 in axonal transport deficits and degeneration using a mice model of acute ocular hypertension (AOHT). We found CD82 exerted the neuroprotective effect through activating mTOR pathway via an intermediate molecule TRAF2. Our findings revealed a novel neuroprotective mechanism and provided therapeutic target for glaucoma treatments.

Materials And Methods

Animals

Male C57BL/6J mice and B6. Cg-*Rptor*$^{tm1.1Dmsa/J}$ (The Jackson Laboratory, 013188) were housed in the Animal Center of the Tongji Medical College. All experimental animals were given free access to food and water in a 12-h light/12-h dark cycle environment. All animals were treated under protocols approved by ARVO Statement for the Use of Animals in Vision and Ophthalmic Research and the institutional IACUC committees of Huazhong University of Science and Technology. Animals of 2-month-old weighing 20-25g were used in all experiments.

Reagents and antibodies

Retinoic acid was obtained from Sigma-Aldrich China (Shanghai, China; R2625). Rapamycin was purchased from MedChemExpress (Shanghai, China; HY-10219). CTB-Alexa 488 and CTB-Alexa 555 were bought from BrainVTA (Wuhan, Hubei, China). The following antibodies were used in western blot: anti-CD82 (ab66400; Abcam; 1:1000); anti-synaptophysin (ab14692; Abcam; 1:1000); anti-p70S6k (2708T; Cell Signaling Technology; 1:1000); anti-p-p70S6k(9234T;Cell Signaling Technology; 1:1000); anti-β-actin (sc-47778; Santa Cruz; 1:1000); anti-TRAF2 (ab126758; Abcam; 1:1000); anti-Raptor (20984-1-AP; Proteintech; 1:1000).The following antibodies were used in immunofluorescence: anti-CD82 (ab66400; Abcam; 1:200); anti-Tuj1 (801201; Biolegend; 1:1000); anti-Iba1(ab48004;Abcam;1:100); anti-GAFP(ab4674; Abcam;1:100); anti-mCherry (ab167453; Abcam; 1:100); anti-synaptophysin (ab14692; Abcam; 1:200); anti-pS6(Ser 240/244)(5364T; Cell Signaling Technology; 1:1000); anti-TRAF2 (ab126758; Abcam; 1:400); anti-Raptor (20984-1-AP; Proteintech; 1:1000); anti-Lamp1 (15665, Cell Signaling Technology; 1:500).

Anti-β-Amyloid (2450; Cell Signaling Technology; 1:100) was used in immunohistochemistry.

Adeno-associated virus administration

rAAV2/9-hsyn-Cd82-2A-mCherry-WPRE-PA, rAAV2/9-hsyn-mCherry-WPRE-PA, rAAV2/9-hsyn-Cre-EGFP-WPRE-PA, rAAV2/9-hsyn-EGFP-WPRE-PA were obtained from BrainVTA (Wuhan, Hubei, China). Each virus preparation contained approximately $2.0x10^{12}$ genome copies/ml. One microliter of AAV was injected in one eye of each animal in the vitreous cavity using a 35-G needle with a 10-μl Hamilton microsyringe (Hamilton, Reno, NV, USA) at a constant rate over 30 s. The needle was held in place for 60 s to allow for intraocular pressure equilibration before removal. Animals were used for subsequent experiments three weeks after AAV injection.

Animal model of Acute Ocular Hypertension

Mouse model of acute glaucoma was performed as previously described(33). Animals undergoing surgery were anesthetized by intraperitoneal injections of 5% chloral hydrate (9 ml/kg). The corneas were topically anesthetized with 0.5% tetracaine hydrochloride, and the pupils were dilated with 1% tropicamide. A 30-gauge infusion needle connected to a standard saline reservoir was used to insert into the anterior chamber of 1 eye. The saline reservoir was elevated to a height of 1.2m for 1 hour. Whitening of the iris and loss of the red reflex suggested the retinal ischemia, and subsequent reperfusion was evident by the red reflex return. The other eye was served as a control with a sham procedure performed without elevating the pressure. After the process, eyes were covered with antibiotic ointment to prevent corneal desiccation and bacterial infection. The animals were allowed to recover for 8, 24, 48, 72 h or 7 days before sacrifice.

Optic nerve crush

Mice were anesthetized by intraperitoneal injections of 5% chloral hydrate (9 ml/kg), and eyes were locally anesthetized using 0.5% tetracaine hydrochloride. A small conjunctival incision was made in the superior posterior area using micro-scissors, and eye muscles were then carefully moved. The optic nerve was exposed intraorbitally and crushed by fine self-closing forceps for 5 s approximately 0.5mm behind the optic disc without damaging the underlying ophthalmic artery. Eyes were covered with antibiotic ointment to protect the cornea after surgery. Mice were euthanized at day 7 post-injury for RGC survival analysis and day 14 or day 28 for axonal regeneration evaluation.

Immunofluorescence

Eyes for retina cross-sectional preparation were fixed in 4% paraformaldehyde (pH= 7.4) as whole globes at RT for 2 days. All specimens were embedded in paraffin to enable ONH to be cut in parallel with ON longitudinal axis. The paraffin-embedded retinal sections (5 μm) were gently washed three times with phosphate-buffered saline (PBS) pre-heated to 37°C and then blocked in 5% donkey serum albumin for 1 hour to avoid nonspecific binding. Afterward, the sections were incubated in diluted primary antibodies at

4℃ overnight. Retinal paraffin sections were washed three times before incubated with the conjugated secondary antibody in 5% bovine serum albumin (RT, 90 min).

Eyes for retinal flat mount were dissected and fixed in 4% paraformaldehyde (pH= 7.4) for 2h at room temperature. The posterior segments of the eye were cut into a ‘petal’ shape with 4 to 5 radial incisions, and then the retinas could be carefully detached. Leave the retinas to cold methanol for at least 20 min to facilitate permeabilization. After rinsed in PBS, retinas were blocked in normal donkey serum for 1h at room temperature and then incubated for 48-72 h at 4℃ with primary antibodies. Afterward, retinas were washed thoroughly in PBS three times and incubated with secondary antibodies at room temperature for 90 min. Finally, retinas were transferred onto slides and mounted with glycerol.

The sections and flat mounts were examined with a laser scanning confocal microscope (Zeiss LSM 710; Zeiss, Oberkochen, Germany) under excitation wavelengths of 405 nm for DAPI, 488 nm for FITC, and 594 nm for cy3, respectively.

For colocalization analysis, Mander’s colocalization coefficient (MCC) was calculated using the ImageJ plugin ’JACoP’.

Evaluation of anterograde axon transport by CTB

Mice were anesthetized by 5% chloral hydrate and mydriasis with 1% tropicamide.1 μl CTB-Alexa 488 (BrainVTA, Wuhan, Hubei, China) was intravitreally injected in one eye using a 10-μl Hamilton microsyringe (Hamilton, Reno, NV, USA). 48h after the injection, animals were anesthetized and sacrificed via cardiac perfusion of normal saline and 4% PFA. Brains and eyes were post-fixed in 4% PFA for an additional 24 h, dehydrated with 30% sucrose in PBS overnight prior to embedding in OCT (Tissue-Tek, Sakura Finetek Inc, Tokyo, Japan). Brains were continuously sliced into 30 μm sections in area of superior colliculus. Eyes were sectioned into 10μm with ONH. Alexa 488 was visualized using a fluorescent microscope (Olympus, Tokyo, Japan).

Axon labeling for regeneration

CTB-Alexa 555 (BrainVTA, Wuhan, Hubei, China) was intravitreally injected 48 h before sacrifice to trace regenerating RGC axons 14- or 28-days post-injury. After 4% PFA perfusion, mice eyes and optic nerves were microdissected and post-fixed for 3 h in 4% PFA. The nerves were dehydrated with 30% sucrose in PBS overnight at 4℃ and embedded in OCT Compound (Tissue-Tek, Sakura Finetek Inc, Tokyo, Japan) for cryosection. Optic nerves were cut longitudinally at a thickness of 10 μm and mounted onto slides. Alexa 555 was imaged using a fluorescent microscope (Olympus, Tokyo, Japan). Regeneration axons were quantified by counting the number of CTB-labeled fibers extended past every 500 μm division from the crush site. The total number of regeneration axons in each optic nerve was estimated using the equation elaborated in the literature(34).

Electron microscopyand analysis

Eyes with optic nerves attached were carefully dissected from the orbit. A 1.5mm section of optic nerve proximal to the globe was isolated and fixed in ice-cold 2.5% glutaraldehyde in 0.1M cacodylate solution. Tissue embedding and ultrathin sectioning were processed as described(35). Sections were examined and photographed with HITACHI H-7000FA TEM.

Axons were classified into three categories according to the condition of the myelin sheath, representing the different degrees of axonal degenerative change. Five non-overlapping visual fields of each section were randomly selected, and the frequency of different degenerative axons was calculated. Observers conducting assessments were masked to the experimental conditions of the images.

Visual FunctionAnalysis

Both eyes were injected with AAV-Cd82 or vehicle three weeks before binocular optic nerve crush. Visual function tests were performed on day 14 and day 28 post-injury. For the dark light preference test, apparatus consisting of a small dark chamber and a large illuminated chamber (550 lumens) with a door allowed mice to move freely for 10 min. The time spent in each compartment was recorded by a camera, and the time ratio was calculated automatically by SuperMaze Software (XinRuan Information Technology, Shanghai). For the optomotor response test, the visual acuity of mice was measured based on an innate visual-motor reflex using a testing chamber(36) and the software OptoTrack from XinRuan Information Technology (Shanghai, China). Mice moved freely on a platform located in the center of an area surrounded by four screens displaying a moving vertical sinusoidal grating pattern. The spatial frequency started from 0.01 to 0.06 cycles per degree with constant rotation speed (12°/s) and 100% contrast to determine the spatial frequency threshold at which the mice still tracked the moving grid. Different testing frequencies occurred randomly and repeated 10 times within one test to reduce the occasional error. Observers were blinded to the group of mice.

Cell culture and transfection

HEK-293T cells were purchased from Boster Biologic Technology. SH-SY5Y cells were given as a gift from the Department of Neurobiology, Tongji Medical College, Huazhong University of Science and Technology.

Cells were maintained in high-glucose DMEM (Hyclone Laboratories, Logan, UT, USA) supplemented with 10% FBS (Gibco, CA, USA) and penicillin (100 U/ml)/streptomycin (100 μg/ml) at 37°C in a humidified atmosphere with air containing 5% CO2. Confluent cell layers were split every three days.

HEK293 and SH-SY5Y cells were transfected with Flag-Cd82 plasmid/vehicle and siTraf2/siNC using Lipofectamine 3000 (Thermo Fisher Scientific) according to the transfection protocol. Cells were cultured for another 48-72 h for further biochemical analyses. Flag-Cd82 plasmid was constructed by cloning the corresponding cDNA into the pcDNA3-Flag vector. TRAF2 siRNA duplexes (5’ -CGACAUGAACAUCGCAAGC-3’) with 30 dTdT overhangs were synthesized at Tsingke biological technology.

Neurite outgrowth assay

RA (all-trans-retinoic acid, Sigma) was used to induce cell differentiation and neurite outgrowth as indicated previously(37). Briefly, SH-SY5Y cells with proper confluence were cultured in 1%FBS medium supplemented with 10μM RA for 7days prior to treatment. On day 4, the medium was replaced with fresh differentiation medium, and on day 7, cells were used for subsequent experiments.

Oxidative stress induced by hydrogen peroxide exposure was indicated to cause axonal degeneration in vitro(38). SH-SY5Y cells were exposed to 100μM hydrogen peroxide for 8h to inhibit neurite outgrowth and recovered in normal medium for another 12h before morphological analysis.

The formation of neurites was observed using an inverted IX71 microscope system (Olympus, Tokyo, Japan). The neurite length of each cell was measured by Image J software plugin 'AxonJ'. The average length of neurites and the ratio of cells with different neurite lengths were analyzed.

Drug handling and administration

Retinoic acid (R2625, Sigma) powder was prepared in DMSO at 3 mg/ml (0.01M) as stock solution and stored in light-protected vials at -80℃. Tissue culture medium was used to dilute the stock solution at a final concentration of 10 μM to induce differentiation of SH-SY5Y cells.

For animal experiments, rapamycin (HY-10219, MedChemExpress) was dissolved in DMSO at 20mg/ml for temporary storage in -20℃. Before each administration, rapamycin stock solution was diluted in sterile saline solution and given intraperitoneally at 6 mg/kg every two days. For cell experiments, rapamycin was dissolved in DMSO at 20mM. Subsequent dilutions were made in growth medium with a final concentration of 100nM and maintained for 2 hours before cells were harvested.

PPI Network visualization

To identify new interaction partners and the corresponding interaction networks between CD82 and mTORC1, we used the online database Molecular Interaction Search Tool (MIST; http://fgrtools.hms.harvard.edu/MIST/)(39)and visualized the protein-protein interaction networks by Cytoscape software 3.8.0(40).

Protein extraction, immunoblots and immunoprecipitation

Cells and tissue from retina, ONH and ON were lysed in RIPA buffer (Applygen Technologies, Beijing China) respectively at designed time-points. BCA Protein Assay Reagent (Boster Biologic Technology) was used to quantify protein concentration. For immunoprecipitation, the same amounts of whole-cell lysate were incubated with the primary antibodies (0.5-2μg) overnight at 4℃. Protein A/G sepharose beads (P2012, Beyotime Biotechnology) were added into the incubation tubes, and the mixture was incubated at 4℃ with gentle shaking for 3 hours. The precipitated complexes were washed five times with RIPA buffer and then mixed with loading buffer (Boster Biologic Technology) and boiled for 5 min. For western blot analysis, equivalent amounts of total protein or immunoprecipitate were fractionated by SDS-PAGE and then transferred to PVDF membrane (MilliporeSigma). Membranes were blocked at room

temperature using 5% nonfat milk in TBST buffer for 1 h and treated overnight at 4°C with diluted primary antibodies. The following day membranes were washed three times with TBST before incubated with horseradish peroxidase-coupled secondary antibodies for 60 min at room temperature. Immunoreactive bands were detected with a chemiluminescence substrate kit (ECLPlus; PerkinElmer Inc, Covina, CA, USA) prior to exposure using either film or digital detection equipment (BLT GelView 6000 pro). Target protein expression levels were quantified using ImageJ software normalized to β-actin or GAPDH level.

RNA isolation and Real-time quantitative PCR

Total RNA was extracted with RNAiso plus (Takara Biomedical Technology, Beijing, China). RNA concentration and quality were assessed on NanoDrop 2000 (Thermo Fisher Scientific). The eligible RNA samples were reverse-transcribed with PrimeScript™RT reagent Kit (RR047A; Takara Biomedical Technology) according to the manufacturer's instructions. The amplified cDNA templates were diluted and used for quantitative PCR with TB GreenPremix Ex Taq (RR420A; Takara Biomedical Technology) on the Applied Biosystems 7300 Real-Time PCR System (Thermo Fisher Scientific). Primer sequences were designed as follows:

Cd82: forward 5'-TGTCCTGCAAACCTCCTCCS-3', reverse5'-CCATGAGCATAGTGACTGCCC-3';

Traf2: forward 5'-GCTCATGCTGACCGAATGTC-3',

reverse 5'- GCCGTCACAAGTTAAGGGGAA-3';

Gapdh: forward 5'-GGAGTCCACTGGCGTCTTCA-3',

reverse 5'- GTCATGAGTCCTTCCACGATACC-3'.

All samples were run in triplicate with blank controls. The relative expression of target genes was calculated by the $2^{-\Delta\Delta CT}$ method with normalization against Gapdh level.

Statistical analysis

The results are expressed by mean ± S.E.M from at least three independent experiments, specific sample size was indicated in the context. Graphing and statistical analysis were performed in statistical software Prism (v.7.03; GraphPad Software, La Jolla, CA, USA). Differences within the experimental groups were assessed by Student's t-test or one-way analysis of variance (ANOVA). P values were considered significant for $P < 0.05$.

Results

1. **CD82 expression was down-regulated in retina, ONH and ON in the early stage after acute ocular hypertension (AOHT) model**

In order to investigate the expression level of CD82 in the posterior segment of eye after IOP elevation, we performed an acute ocular hypertension (AOHT) mouse model by elevating the IOP to 75 mm Hg for 1h. This model was suitable for studying the very early events after IOP spike because of the controllable IOP elevation and duration. The protein level of CD82 in retina, unmyelinated optic nerve head (ONH), and the posterior myelinated optic nerve (ON) was detected at 8h, 1d, 2d, 3d and 7d after AOHT by immunofluorescence staining. As shown in Figure 1a, results were similar across all three sites that CD82 immunofluorescence started to decline as early as 8h and reached the lowest at 2d, partially recovering at 7d. The further western blotting analysis confirmed that CD82 protein level was downregulated at 8h and 2d compared to the control groups, with a certain degree of recovery on day 7 (Figure 1, b-e). These results elucidated the temporal expression pattern of CD82 after AOHT, indicating the possible involvement of CD82 in the process of optic nerve injury after ocular hypertension insults.

Next, we turn to explore the cellular localization of CD82 in posterior segment of the eye. Immunofluorescent double-labeling of CD82 with the cell markers of RGC (Tuj1), microglia (Iba1), and astrocyte (GAFP) was performed (Figure 1f-h). It was apparent that CD82 mainly localized parallel to RGC markers Tuj1 but rarely co-labeled with Iba1 or GAFP, whether modeling or not, suggesting that CD82 mainly functioned in RGCs and their axons rather than in other glial cells. These results further confirmed the spatial expression pattern of CD82, determined that CD82 directly acted on RGCs and their axons in the pathological process after ocular hypertension.

2. **CD82 overexpression in retina and ON was achieved by Intravitreal injection of recombinant adeno-associated virus rAAV2/9-Cd82-mCherry**

To investigate the role of CD82 in the ocular hypertension mouse model, an adeno-associated virus vector was designed to overexpress CD82 in mouse retina. The rAAV2/9-Cd82-mCherry or rAAV2/9-mCherry (vehicle) was intravitreally injected 28d before mice were sacrificed, and CD82 protein overexpression efficiency was verified by immunofluorescence as well as western blotting analysis. As seen in Figure 2a, it was evident that CD82 immunofluorescence intensity was much higher in AAV-Cd82 injection group than vehicle or control groups, covering retina, ONH and particularly pronounced in the optic nerve. The results of western blotting also revealed a satisfactory transfection efficiency (Figure 2b, c). Immunofluorescence of the virus tag mCherry co-labeled with Tuj1 was presented in Supplemental 1.

3. **CD82 overexpression protected against axonal transport deficits after AOHT.**

Here we focused on the lesions in ONH, which is the critical site in glaucoma optic neuropathy(41), as well as the superior colliculus (SC), which is the primary projection site for RGCs in the rodent brain (3).

First, we visualized the anterograde transport function of the optic nerve by intraocular injection of cholera toxin β-subunit (CTB), which labeled the entire retinal projection via active uptake and transport (Figure 3a, b). Sections of ONH presented that CTB was uniformly distributed along the entire axon length (>2000μm) in sham group. At the same time, after inducing AOHT, CTB was failed to be transported distantly, with a severe obstacle on day 2 (<200μm) and slightly recovered on day 7 (Figure 3c, d).

Notably, CD82 overexpression reversed such obstruction and maintained the CTB labeling distance to over 400μm on day 2.

CTB signal density in SC was demonstrated in three layers as rostral, middle, and caudal from consecutive serial sections to show disruption of transport reaching the brain 2 days after AHOT modeling. In control group, SC had a complete CTB distribution, reflecting entire retinotopic transportation to SC (Figure 3e). While in the AOHT group, there was a heterogeneous distribution of CTB signals with massive deficits in all three layers. In contrast, SC from AOHT mice with AAV-Cd82 injection manifested few losses of CTB labeling.

Next, we evaluated endogenous cargo transport by immunofluorescence staining of Synaptophysin, a vesicular transport marker synthesized by RGCs and anterogradely transported along ON. In normal conditions, there was no protein accumulation in ONH. However, synaptophysin protein was initiated to deposit at ONH within 8h after the AOHT model and peaked at 2d, similar to the foregoing cases**.** While in AAV-Cd82 injection group, such accumulation was alleviated, suggesting a potential protective effect of CD82 against axonal transport deficits (Figure 3f). Proteins extracted from ONH were performed for western blotting analysis. An increase of synaptophysin protein in ONH was evident after modeling, and the protective effect of CD82 was also verified (Figure 3g-j).

4. **CD82 overexpression protected optic nerve from axonal degeneration induced by AOHT**

Optic nerve axonal degeneration was the following pathological event due to axonal transport deficits, which was more severe and hard to reverse. Here we detected the axonal degeneration changes of the optic nerve after AOHT.

First, we evaluated the axon loss in retina whole mount by immunofluorescence staining of Tuj1 (Figure 4a). Radial cord-like immunofluorescence staining in the nerve fiber layer demonstrated the axons of ganglion cells. Axon loss occurred in the AOHT group, showing weakened immunofluorescence and sparser axon distribution. With CD82 overexpression, the axon distribution was nearly intact (Figure 5b). However, there was no significant loss of RGC soma yet at this stage, indicating the axonal degeneration to be an early pathological change prior to RGC death (Figure 5c). The existent time-lag between earlier axon loss and later RGC body death was consistent with previous findings(42).

Electron microscopy was able to show the ultrastructural features of RGC axonal degeneration, identified by swollen axonal profiles, disorganized neurofilaments, collapsed myelin sheaths and swollen mitochondria(42). Here, we observed the pathological changes of the optic nerve ultrastructure caused by high IOP. Representative images from control, AOHT and CD82 intervention groups were displayed in Figure 4d. In normal group, there were compact layers of myelin lamellae surrounding the axons. However, two days after AOHT, myelinated axons appeared to be delaminated with intramyelinic lacunae or vacuoles. Myelin debris and axonal swellings were frequently observed, emergence of almost collapsed axon structure with multilayered whorled masses indicating axon towards the end stage of degeneration. In order to quantify the degree of damage, the proportion of axons with normal, loosen, or

decompacted myelin was calculated (Figure 4e). In AOHT group, the majority of the myelin sheath was loosened, with another considerable fraction to be decompacted. With CD82 overexpression, such impairment was alleviated and close to normal.

Extensive studies have revealed that β-amyloid precursor protein (Aβ) was involved in glaucomatous neuropathology(45), and emerged as a hallmark of neurodegeneration(46, 47). Next, we applied Aβ immunohistochemical staining on optic nerve cross-sections to evaluate axonal degeneration after ocular hypertension. The acute axonal injury was demonstrated by prominent Aβ immunoreactivity and focal immunopositive distribution. As shown in Figure 4f-g, axons immunoreactive for Aβ were present to a significantly lower degree in CD82 overexpression mice than the vehicle-treated group after modeling, indicating the CD82 overexpression be an effective neuroprotection intervention.

To further verify the protective effect of CD82 overexpression in vitro, we used Retinoic acid (RA)-differentiated SH-SY5Y cells to simulate mature neurons like RGCs(48). With 10μM RA stimulation for 7days, SH-SY5Y cells differentiated and possessed characteristic neuronal morphology with long, extensively branched neurites. H_2O_2 (100 μM) was applied to imitate cell injury in retinal degeneration(38), and CD82 overexpression was achieved by Cd82-plasmid transfection (Figure 4h). As seen in Figure 4i, H_2O_2 inhibited the RA-induced neurite outgrowth and led to the cell process retraction. When cells were transfected with Cd82-plasmid before H_2O_2 injury, the axonal outgrowth was almost restored to the normal state. The quantitative data in Figure 4j-k showed the average length of neurites and the proportion of the cells with different neurite lengths in each group, indicating that H_2O_2 inhibited RA-induced outgrowth of axon-like cell processes in SH-SY5Y cells, while CD82 overexpression could partially reverse this effect, thus played a role in neuroprotection.

5. **CD82 overexpression promoted axon regeneration, RGC survival, and visual function after optic nerve crush (ONC) model**

Experiments above exhibited that CD82 was capable of improving axonal transport and subsequently protected against axonal degeneration after acute IOP hypertension, which was considered to be a relatively moderate model with mild anatomic changes. Currently, there were limited means to reverse optic nerve damage and restore eyesight in late-stage glaucoma with extensive axonal injury and RGC loss(49). Here we induced CD82 overexpression in a more dramatic injury model, namely optic nerve crush (ONC), which led to evident neuronal loss and rapid axonal damage by directly interrupting axoplasmic transport(50) comparable to advanced glaucoma.

AAV-Cd82 was intravitreally injected 2 weeks before ONC, and the optic nerve was allowed to regenerate for 14 or 28 days. CTB was intravitreally injected 2 days before mice were sacrificed to label regenerating axons (Figure 5a). Figure 5b presented the typical images of CTB-traced axon regeneration after ONC. Regenerating and sprouting RGC axon fibers extended over 1 mm beyond the crush site at day 14 and extended to 2 mm at day 28 under the condition of CD82 overexpression, with no visible regeneration in the injury-only group regardless of recovery time (Figure 5c). In addition, RGC survival was evaluated by

RBPMS immunofluorescence staining in retina flat mounts 7 days after ONC (Figure 5d). Promotion of RGC survival upon CD82 overexpression was significant in the central retina, while the effect in the peripheral area was not so evident (Figure 5e, f).

We then tested whether CD82 overexpression could restore the function of RGCs through mouse visual function tests. Dark/light preference tests were performed to measure the light perception (LP) of mice with bilateral ONC with or without AAV-Cd82 injection, in which a reduced duration in the dark compartment reflected a loss of vision (Figure 5g). Tests revealed that the ratio of time in light/dark was increased after ONC and recovered significantly in CD82 overexpression group at both time points, indicating a restoration of LP after treatment with CD82 (Figure 5h). High-contrast visual stimulation was performed to measure the optomotor response, reflecting the visual acuity of mice (Figure 5i). High spatial frequency threshold indicated improved visual acuity in AAV-Cd82 injected mice compared to the injury-only group at day 28 after bilateral ONC (Figure 5j). Overall, the restored vision-dependent behavior of mice following CD82 overexpression demonstrated its ability to improve visual function after optic nerve injury.

6. **CD82 overexpression protected against axonal transport deficits through a mTORC1-dependent mechanism**

The mTOR signaling pathway was critical in regulating neuronal function. We next asked whether the mTOR pathway was required for CD82 mediated protection effects. Here we induced cell injury via the addition of H_2O_2 and overexpressed CD82 by plasmid transfection in HEK-293T cells. Western blotting analysis in Figure 6A showed that phosphorylated-pS6K, an indicator of mTORC1 pathway activation, was down-regulated in H_2O_2-treated cells while recovered following CD82 overexpression (Figure 6a, b). Furthermore, CD82-induced increase of phosphorylated-pS6K could be blocked by rapamycin, a potent and specific inhibitor of mTOR, confirming the participation of mTORC1 pathway downstream of CD82 (Figure 6c, d). These regulatory relations could also be corroborated in retina tissues as shown in Figure 6e. Double-immunofluorescence staining in retina flat mount of phosphorylated-S6, a substrate downstream of p70S6K, with RGC marker Tuj1, was decreased in AOHT group, while CD82 overexpression could prevent such decline. Treatment of rapamycin diminished the signal activation effect of CD82.

To further validate the role of mTORC1 activity in regulating axonal transport function promoted by CD82, we repeated previous experiments with the addition of rapamycin treatment every two days for 28 days to block mTOR activity in vivo. In this case, overexpression of CD82 failed to relieve the axonal transport deficits induced by AOHT, manifested in accumulation of synaptophysin protein at ONH (Figure 6h), as well as the impairment of CTB transport from eye to SC (Figure 6 f, g). Considering the confounding effect of the pharmacological inhibitor Rapamycin due to systemic drug administration and low tissue-specificity, we used the conditional knockout mouse to target RGCs by injecting AAV-*hsyn-cre* into the vitreous body of *Rptor*$^{fl/fl}$mice to delete Raptor, the exclusive function component of mTORC1, to verify the specific effect of mTORC1 pathway in RGCs (Figure 6i). The results of the species identification and

the Raptor knockdown efficiency in retina were shown in Supplemental 2. Figure 6j-k illustrated the deactivation of the mTORC1 pathway in Cre injected eyes from *Rptor*$^{fl/fl}$mice with or without CD82 overexpression. Assessment of axonal transport in Figure 6l-n was consistent with the previous results that inhibition of mTORC1 activity in RGCs blocked the protective effects of CD82.

7. **CD82 activated mTORC1 via TRAF2 mediated k63-linked ubiquitylation to protect against neurodegeneration.**

The molecular pathway by which CD82 influences mTORC1 activation was next addressed. We utilized the Molecular Interaction Search Tool (MIST) database to extract hub molecules connected CD82 with mTORC1 from the protein-protein interaction (PPI) network. The consequent protein Interaction map was visualized by Cytoscape software. Node size reflected the compositive correlation of the candidate proteins to CD82 and mTOR. As demonstrated in Figure 7a, Tumor necrosis factor receptor associated factor 2 (TRAF2) stood out to be the most likely intermediate molecules due to its direct association with both target proteins (Figure 7b). We then examined the mRNA level of Traf2 in H_2O_2-treated HEK-293T cells with or without CD82 overexpression by RT-PCR. The level of Traf2 mRNA was down-regulated by H_2O_2 stimulation and recovered with CD82 overexpression (Figure 7c). Further western blotting analysis of TRAF2 protein level was consistent with PCR results (Figure 7d, e), indicating that CD82 overexpression caused up-regulation of TRAF2. To verify our ex vivo findings in vivo, we evaluated the expression of TRAF2 in mouse model of AOHT with and without AAV-Cd82 injection. Figure 7f provides the immunofluorescence staining of TRAF2 with Tuj1 in retinal sections from different groups. Expression of TRAF2 in Tuj1-positive GCL was markedly decreased, while CD82 overexpression suppressed this decline. Results above indicated TRAF2 as a downstream effector regulated by CD82.

Impacts of CD82 induced up-regulation of TRAF2 on mTORC1 activation was next explored by western blotting assessment of phosphorylated-pS6K. CD82 overexpression led to increased protein level of TRAF2, in turn, activated the mTORC1 pathway (Figure 7g, h). To validate whether CD82 induced activation effect was dependent on TRAF2, we used siRNA to knockdown Traf2 in Cd82 overexpression cells. Upon knockdown of Traf2, CD82 was no longer capable of activating the downstream phosphorylation of pS6K (Figure 7g, h), indicating a TRAF2-dependent manner underlying CD82 induced effect.

It has been demonstrated that K63-linked ubiquitination regulated the activity of mTORC1(51, 52). This motivated us to speculate TRAF2 mediated K63-linked ubiquitination participating in mTORC1 activation. Therefore, we detected the K63-linked ubiquitination status of RAPTOR, the specific components of mTORC1, using anti-ubiquitin (linkage-specific K63) antibody by immunoprecipitation. As shown in Figure 7i, high level of K63-linked ubiquitination was exhibited in CD82 overexpression cells compared to control group, which was attenuated by siTraf2 transfection. This made us confident that CD82 acted through upregulating TRAF2, which was capable of ubiquitinating RAPTOR to govern mTORC1 activation. Further co-Immunofluorescence analysis demonstrated an increased colocalization of

RAPTOR with the lysosomal marker LAMP-1 in CD82 overexpression SH-SY5Y cells, which was reduced in siTraf2 transfected cells (Figure 7j, k).

Finally, we tested the effect of TRAF2 on neurodegenerative pathology with neurite outgrowth assay. Figure 7l-n presented that CD82 induced outgrowth-promoting capability was retarded by siTraf2, confirming that CD82 protected against neurodegeneration through positive regulation of TRAF2.

Collectively, CD82 activated mTORC1 through TRAF2 mediated ubiquitylation to protect against optic nerve injury. TRAF2 was decreased in RGCs after AOHT while maintained the level in CD82 overexpression eyes. Interference of Traf2 by siRNA reduced the K63-ubiquitin of RAPTOR, subsequently influenced its lysosomal positioning and further activation.

Discussion

Altogether, our study revealed the protective effect of CD82 against axonal transport deficits and subsequent axon degeneration after acute ocular hypertension (AOHT). Intravitreally injection of AAV-Cd82 could efficiently overexpress CD82 in RGCs and upregulated TRAF2, which activates mTORC1 through K63-linked ubiquitylation and intracellular repositioning of Raptor (Figure 8). Additionally, the protective effect was also verified in an ONC model to promote axonal regeneration, indicating a potent role of CD82 in neuroprotection.

Our study demonstrated spatial characteristics and the timeframes of the key early pathological events in an acute glaucoma model. Axonal transport impairment initiated at the ONH and progressed to involved the brain (i.e., superior colliculus), which occurred as early as 8h after IOP elevation, reached the highest level at day 2 and then gradually declined. Such spontaneous recovery was insufficient to successfully reverse the subsequent axonal degeneration, at which point the RGC soma still remained intact. The pathological progression in this study was basically consistent with previous research using other glaucoma model(53, 54). Studies using spontaneous or laser-induced rodent model of glaucoma showed that anterograde transport was disrupted earliest after increased IOP, followed by retrograde transport depletion, axonal degeneration appeared subsequently (41). In addition, an intervention restoring axonal transport preserved RGC axon structure and vision function damaged in DBA/2J and microbead occlusion model, indicating axonal transport as an early and promising therapeutic target in glaucoma(55). A more recent study using Dex-induced ocular hypertension demonstrated axonal transport deficits and axonal degeneration preceding RGC structural and functional loss. Partial block of axonal transport was associated with early stages of optic nerve degeneration(56). However, the axonal transport deficits in such research were progressively aggravated due to sustained IOP elevation, making it difficult to inquire and intervene the early reversible alterations. By inducing AOHT at stable level of 75mmHg for 1h, we found the transport deficits still reversible at this condition, while axonal degeneration was already initiated. Hence, early interventions of axonal transport function are more meaningful to protect against the irreversible end-stage neuropathy in glaucoma. As far as we concerned,

the chronology of pathological events has not yet been reported in an acute glaucoma model, with an even higher IOP amplitude in a rapid time course as applied in our study.

Here we identified the protective effect of CD82 in promoting axonal transport and subsequently protecting against neurodegeneration in AOHT model. Of concern was the variation trend of CD82 protein level consistent with the severity of axonal transport disorders after AOHT. In other words, reduced CD82 level corresponded to the aggravated axonal dysfunction with time synchronization after injury. The spatial localizations of CD82 mainly in RGCs and their axons further indicated its direct role in regulating RGC axonal functions. Given this, we applied AAV mediated Cd82 overexpression specific in RGCs as a complementary gene therapy. Such treatment was effective in improving the prognosis of glaucomatous axonopathy in mouse model of AOHT. In addition, we illustrated the pro-regenerative effects of CD82 in a more severe injury model of ONC, in which the axon loss and RGC death was apparent due to complete axoplasmic flow disruption, which was comparable to advanced glaucoma. Upon AAV-Cd82 injection, axon regeneration and vision restoration were achieved 28 days after injury. Such extent of recovery was about the same as other reported pro-regenerative strategies. So far, most of these means were oriented towards improving different neuron intrinsic capacities, such as targeting key signaling pathways(57, 58), manipulating transcription factors (48), and regulating epigenetic mechanisms(59). Otherwise, promoted axonal transports have been proved to increase axonal regeneration in many studies. Zhou et al. found that enhanced mitochondrial transport in snph knockout mice could promote axonal regeneration in a sciatic nerve crush model(60). Xiong et al. induced disrupted axonal transport using a Glued^{DN} mutation in *Drosophila melanogaster* resulting in a strong inhibition to the axonal regenerative response(61). Eva et al. revealed that inactivated ARF6 could enhance integrin and Rab11 transport thus leading to axonal regeneration after a laser axotomy model(62). Here we confirmed pro-regeneration effect of CD82 in mouse ONC model, which could be partly due to enhancement of axonal transport demonstrated above.

Our data showed that CD82 overexpression reverted the decline of p-pS6k induced by injury, indicating the activation of mTORC1 underlying the protection effect. The mTOR pathway has been reported to function downstream of virous signaling molecules to promote axonal regeneration(34, 63-65) . The PPI data obtained from the Database of MIST suggested a mediating role of TRAF2 between CD82 and mTORC1 pathway. A recent study indicated that K63-linked polyubiquitination was critical for mTORC1 activation and proved that TRAF6 mediated mTORC1 translocation to the lysosome for subsequent activation (30). Another research on TRAF2 also emphasized its role in ubiquitination of mTOR components to maintain the balanced homeostasis of mTORC1 and mTORC2 activation(66). Here we demonstrated a novel mechanism that TRAF2 functioned downstream of CD82 to activated mTORC1 through ubiquitinating Raptor. However, the mechanisms of how CD82 upregulated TRAF2 remains to be elucidated.

CD82, also named Tspan27, is a member of the tetraspanin superfamily characterized by four transmembrane domains. As membrane scaffold proteins, tetraspanins are proposed to organize plasma membrane topology thus regulate many biological processes (10,11). However, current research about the tetraspanin CD82 is mainly focused on tumor metastasis regulation and immune recognition(67, 68).

Its function in other physiological and pathophysiological processes remains largely unknown. Research on tetraspanin function in nervous system is still at an early stage, however, gradually some evidence has emerged to indicate roles of other tetraspanins in regulation of nervous system. TspanC8 subgroup (Tspan5, 10, 14, 15, 17, and 33) was found to interact with ADAM10 to regulate development of the nervous system(69, 70). Tspan2 was involved in the differentiation of oligodendrocyte into myelin-forming glia(71). Tspan6 and 7 participated in regulating glutamatergic transmission and synaptic formation(72). Tspan22 and another tetraspanin ROM1 functioned in development of photoreceptor outer segments, which were the organelle specialized for visual transduction(73). As far as we concerned, our study was the first to explore the role of CD82 in neurodegeneration disease in eyes, which helped to fill the gap and gain deeper insights into tetraspanins, as well as provide potential neuroprotective strategy in optic nerve protection.

Conclusions

In conclusion, our studies reveal that axonal transport deficits come out at early stage of glaucomatous optic nerve degeneration, preceding RGC structural loss. CD82 expression level is downregulated during this process. Overexpression of CD82 with AAV vector improves axonal transports and relieves axonal degeneration both in vivo and in vitro. In addition, another mouse model of ONC indicates that CD82 overexpression could stimulate optic nerve regeneration and restore mouse vision during more dramatic ON injury, suggesting a universal protective effect of CD82. The underlying mechanism for this process is demonstrated in our study that CD82 activates mTORC1 pathway through TRAF2 mediated K63-ubiquitination of raptor. Hence, our findings provide a complete perspective of the neuroprotection effect of CD82, which reveal a novel neuroprotective mechanism and help to guide treatment of glaucoma.

Abbreviations

RGC: retinal ganglion cell

ON: optic nerve

IOP: intraocular pressure

ONH: optic nerve head

mTOR: mechanistic target of rapamycin

BDNF: brain-derived neurotrophic factor

pS6K: p70-S6 ribosomal protein kinase

p-S6: phospho-S6 ribosomal protein

TRAF: tumor necrosis factor (TNF) receptor associated factor

AOHT: acute ocular hypertension

AAV: adeno-associated virus

SC: superior colliculus

CTB: cholera toxin β-subunit

Aβ: β-amyloid precursor protein

RA: retinoic acid

ONC: optic nerve crush

MIST: Molecular Interaction Search Tool

PPI: protein-protein interaction

Tspan: tetraspanin

Declarations

Availability of data and materials

Further information and requests for reagents and data may be directed and will be fulfilled by the corresponding author Yin Zhao (Email: zhaoyin85@hust.edu.cn).

Acknowledgements

Not applicable.

Funding

The current studies were supported by funding from the National Natural Science Foundation of China Grant Nos.31800868 and Tongji Hospital (HUST) Foundation for Excellent Young Scientist Grant No. 2020YQ18 (to Dr Yin Zhao). National Natural Science Foundation of China Grant Nos.81770921, 82070965 (to Dr Hong Zhang).

Author Contributions

Y.Z, and H.Z conceived and designed the project; M.Y and JQ.H performed the experiments; M.Y and JQ.H wrote the manuscript; J.L, QX.M, YY.H, XT. L, K.Y, BW. Z, QM. D, X.L helped to revise the manuscript. All authors read and approved the final manuscript.

Ethics declarations

Ethics approval and consent to participate

Ethics approvals are in place for the animal work carried out in this work.

Competing interests

No biomedical financial interests or potential conflicts of interest exist.

References

1. Jonas JB, Aung T, Bourne RR, Bron AM, Ritch R, Panda-Jonas S. Glaucoma. Lancet (London, England). 2017;390(10108):2183-93.
2. Calkins DJ. Critical pathogenic events underlying progression of neurodegeneration in glaucoma. PROG RETIN EYE RES. 2012;31(6):702-19.
3. Crish SD, Sappington RM, Inman DM, Horner PJ, Calkins DJ. Distal axonopathy with structural persistence in glaucomatous neurodegeneration. P NATL ACAD SCI USA. 2010;107(11):5196-201.
4. Shirendeb UP, Calkins MJ, Manczak M, Anekonda V, Dufour B, McBride JL, et al. Mutant huntingtin's interaction with mitochondrial protein Drp1 impairs mitochondrial biogenesis and causes defective axonal transport and synaptic degeneration in Huntington's disease. HUM MOL GENET. 2012;21(2):406-20.
5. Nicolas A, Kenna KP, Renton AE, Ticozzi N, Faghri F, Chia R, et al. Genome-wide Analyses Identify KIF5A as a Novel ALS Gene. NEURON. 2018;97(6):1268-83.
6. Godena VK, Brookes-Hocking N, Moller A, Shaw G, Oswald M, Sancho RM, et al. Increasing microtubule acetylation rescues axonal transport and locomotor deficits caused by LRRK2 Roc-COR domain mutations. NAT COMMUN. 2014;5:5245.
7. Adalbert R, Milde S, Durrant C, Ando K, Stygelbout V, Yilmaz Z, et al. Interaction between a MAPT variant causing frontotemporal dementia and mutant APP affects axonal transport. NEUROBIOL AGING. 2018;68:68-75.
8. Quigley HA, Addicks EM, Green WR, Maumenee AE. Optic nerve damage in human glaucoma. II. The site of injury and susceptibility to damage.; 1981. p. 635-49.
9. Quigley HA, McKinnon SJ, Zack DJ, Pease ME, Kerrigan-Baumrind LA, Kerrigan DF, et al. Retrograde axonal transport of BDNF in retinal ganglion cells is blocked by acute IOP elevation in rats. INVEST OPHTH VIS SCI. 2000;41(11):3460-6.
10. Boucheix C, Rubinstein E. Tetraspanins. Cellular and molecular life sciences : CMLS. 2001;58(9):1189-205.
11. Hemler ME. Tetraspanin functions and associated microdomains. Nature reviews. Molecular cell biology. 2005;6(10):801-11.
12. Bassani S, Cingolani LA, Valnegri P, Folci A, Zapata J, Gianfelice A, et al. The X-linked intellectual disability protein TSPAN7 regulates excitatory synapse development and AMPAR trafficking.

NEURON. 2012;73(6):1143-58.

13. Usardi A, Iyer K, Sigoillot SM, Dusonchet A, Selimi F. The immunoglobulin-like superfamily member IGSF3 is a developmentally regulated protein that controls neuronal morphogenesis. DEV NEUROBIOL. 2017;77(1):75-92.
14. Kohl S, Giddings I, Besch D, Apfelstedt-Sylla E, Zrenner E, Wissinger B. The role of the peripherin/RDS gene in retinal dystrophies. Acta anatomica. 1998;162(2-3):75-84.
15. Dong JT, Lamb PW, Rinker-Schaeffer CW, Vukanovic J, Ichikawa T, Isaacs JT, et al. KAI1, a metastasis suppressor gene for prostate cancer on human chromosome 11p11.2. Science (New York, N.Y.). 1995;268(5212):884-6.
16. Albert V, Hall MN. mTOR signaling in cellular and organismal energetics. CURR OPIN CELL BIOL. 2015;33:55-66.
17. Lipton JO, Sahin M. The neurology of mTOR. NEURON. 2014;84(2):275-91.
18. Harun-Or-Rashid M, Pappenhagen N, Palmer PG, Smith MA, Gevorgyan V, Wilson GN, et al. Structural and Functional Rescue of Chronic Metabolically Stressed Optic Nerves through Respiration. The Journal of neuroscience : the official journal of the Society for Neuroscience. 2018;38(22):5122-39.
19. Yang X, Hondur G, Li M, Cai J, Klein JB, Kuehn MH, et al. Proteomics Analysis of Molecular Risk Factors in the Ocular Hypertensive Human Retina. INVEST OPHTH VIS SCI. 2015;56(10):5816-
20. Ishizuka Y, Kakiya N, Witters LA, Oshiro N, Shirao T, Nawa H, et al. AMP-activated protein kinase counteracts brain-derived neurotrophic factor-induced mammalian target of rapamycin complex 1 signaling in neurons. J NEUROCHEM. 2013 2013-01-01;127(1):66-77.
21. Losiewicz MK, Elghazi L, Fingar DC, Rajala RVS, Lentz SI, Fort PE, et al. mTORC1 and mTORC2 expression in inner retinal neurons and glial cells. EXP EYE RES. 2020;197:108131.
22. Pan S, Zhan S, Pan Y, Liu W, Bian L, Sun B, et al. Tetraspanin 8-rictor-integrin α3 complex is required for glioma cell migration. INT J MOL SCI. 2015;16(3):5363-74.
23. Cho JH, Kim E, Son Y, Lee D, Park YS, Choi JH, et al. CD9 induces cellular senescence and aggravates atherosclerotic plaque formation. CELL DEATH DIFFER. 2020;27(9):2681-96.
24. Zismanov V, Drucker L, Attar-Schneider O, Matalon ST, Pasmanik-Chor M, Lishner M. Tetraspanins stimulate protein synthesis in myeloma cell lines. J CELL BIOCHEM. 2012;113(7):2500-
25. Yang X, Sun S. Targeting signaling factors for degradation, an emerging mechanism for TRAF functions. IMMUNOL REV. 2015;266(1):56-71.
26. Dhillon B, Aleithan F, Abdul-Sater Z, Abdul-Sater AA. The Evolving Role of TRAFs in Mediating Inflammatory Responses. FRONT IMMUNOL. 2019;10:104.
27. Silke J, Brink R. Regulation of TNFRSF and innate immune signalling complexes by TRAFs and cIAPs. CELL DEATH DIFFER. 2010;17(1):35-45.
28. Ikeda F, Crosetto N, Dikic I. What determines the specificity and outcomes of ubiquitin signaling? CELL. 2010;143(5):677-81.

29. Mukhopadhyay D, Riezman H. Proteasome-independent functions of ubiquitin in endocytosis and signaling. Science (New York, N.Y.). 2007;315(5809):201-5.
30. Linares JF, Duran A, Yajima T, Pasparakis M, Moscat J, Diaz-Meco MT. K63 polyubiquitination and activation of mTOR by the p62-TRAF6 complex in nutrient-activated cells. MOL CELL. 2013;51(3):283-96.
31. Ghosh P, Wu M, Zhang H, Sun H. mTORC1 signaling requires proteasomal function and the involvement of CUL4-DDB1 ubiquitin E3 ligase.; 2008. p. 373-81.
32. Hussain S, Feldman AL, Das C, Ziesmer SC, Ansell SM, Galardy PJ. Ubiquitin hydrolase UCH-L1 destabilizes mTOR complex 1 by antagonizing DDB1-CUL4-mediated ubiquitination of raptor. MOL CELL BIOL. 2013;33(6):1188-97.
33. Chi W, Li F, Chen H, Wang Y, Zhu Y, Yang X, et al. Caspase-8 promotes NLRP1/NLRP3 inflammasome activation and IL-1β production in acute glaucoma. P NATL ACAD SCI USA. 2014;111(30):11181-6.
34. Park KK, Liu K, Hu Y, Smith PD, Wang C, Cai B, et al. Promoting axon regeneration in the adult CNS by modulation of the PTEN/mTOR pathway. Science (New York, N.Y.). 2008;322(5903):963-6.
35. Alavi MV, Bette S, Schimpf S, Schuettauf F, Schraermeyer U, Wehrl HF, et al. A splice site mutation in the murine Opa1 gene features pathology of autosomal dominant optic atrophy. Brain : a journal of neurology. 2007;130(Pt 4):1029-42.
36. Kretschmer F, Kretschmer V, Kunze VP, Kretzberg J. OMR-arena: automated measurement and stimulation system to determine mouse visual thresholds based on optomotor responses. PLOS ONE. 2013;8(11):e78058.
37. Lopes FM, da Motta LL, De Bastiani MA, Pfaffenseller B, Aguiar BW, de Souza LF, et al. RA Differentiation Enhances Dopaminergic Features, Changes Redox Parameters, and Increases Dopamine Transporter Dependency in 6-Hydroxydopamine-Induced Neurotoxicity in SH-SY5Y Cells. NEUROTOX RES. 2017;31(4):545-59.
38. Fang C, Bourdette D, Banker G. Oxidative stress inhibits axonal transport: implications for neurodegenerative diseases. MOL NEURODEGENER. 2012;7:29.
39. Hu Y, Vinayagam A, Nand A, Comjean A, Chung V, Hao T, et al. Molecular Interaction Search Tool (MIST): an integrated resource for mining gene and protein interaction data. NUCLEIC ACIDS RES. 2018;46(D1):D567-74.
40. Shannon P, Markiel A, Ozier O, Baliga NS, Wang JT, Ramage D, et al. Cytoscape: a software environment for integrated models of biomolecular interaction networks. GENOME RES. 2003;13(11):2498-504.
41. Chidlow G, Ebneter A, Wood JPM, Casson RJ. The optic nerve head is the site of axonal transport disruption, axonal cytoskeleton damage and putative axonal regeneration failure in a rat model of glaucoma. ACTA NEUROPATHOL. 2011;121(6):737-51.
42. Kalesnykas G, Oglesby EN, Zack DJ, Cone FE, Steinhart MR, Tian J, et al. Retinal ganglion cell morphology after optic nerve crush and experimental glaucoma. INVEST OPHTH VIS SCI. 2012;53(7):3847-57.

43. Saggu SK, Chotaliya HP, Blumbergs PC, Casson RJ. Wallerian-like axonal degeneration in the optic nerve after excitotoxic retinal insult: an ultrastructural study. BMC NEUROSCI. 2010;11:97.
44. Payne SC, Bartlett CA, Harvey AR, Dunlop SA, Fitzgerald M. Myelin sheath decompaction, axon swelling, and functional loss during chronic secondary degeneration in rat optic nerve. INVEST OPHTH VIS SCI. 2012;53(10):6093-101.
45. Ito Y, Shimazawa M, Tsuruma K, Mayama C, Ishii K, Onoe H, et al. Induction of amyloid-β(1-42) in the retina and optic nerve head of chronic ocular hypertensive monkeys. MOL VIS. 2012;18:2647-
46. You Y, Joseph C, Wang C, Gupta V, Liu S, Yiannikas C, et al. Demyelination precedes axonal loss in the transneuronal spread of human neurodegenerative disease. Brain : a journal of neurology. 2019;142(2):426-42.
47. Kipfer-Kauer A, McKinnon SJ, Frueh BE, Goldblum D. Distribution of amyloid precursor protein and amyloid-beta in ocular hypertensive C57BL/6 mouse eyes. CURR EYE RES. 2010;35(9):828-34.
48. Lu Y, Brommer B, Tian X, Krishnan A, Meer M, Wang C, et al. Reprogramming to recover youthful epigenetic information and restore vision. NATURE. 2020;588(7836):124-9.
49. Roska B, Sahel J. Restoring vision. NATURE. 2018;557(7705):359-67.
50. Vidal-Sanz M, Galindo-Romero C, Valiente-Soriano FJ, Nadal-Nicolás FM, Ortin-Martinez A, Rovere G, et al. Shared and Differential Retinal Responses against Optic Nerve Injury and Ocular Hypertension. FRONT NEUROSCI-SWITZ. 2017;11:235.
51. Senft D, Qi J, Ronai ZA. Ubiquitin ligases in oncogenic transformation and cancer therapy. Nature reviews. Cancer. 2018;18(2):69-88.
52. Jiang Y, Su S, Zhang Y, Qian J, Liu P. Control of mTOR signaling by ubiquitin. ONCOGENE. 2019;38(21):3989-4001.
53. Dengler-Crish CM, Smith MA, Inman DM, Wilson GN, Young JW, Crish SD. Anterograde transport blockade precedes deficits in retrograde transport in the visual projection of the DBA/2J mouse model of glaucoma. FRONT NEUROSCI-SWITZ. 2014;8:290.
54. Buckingham BP, Inman DM, Lambert W, Oglesby E, Calkins DJ, Steele MR, et al. Progressive ganglion cell degeneration precedes neuronal loss in a mouse model of glaucoma.; 2008. p. 2735-44.
55. Bond WS, Hines-Beard J, GoldenMerry YL, Davis M, Farooque A, Sappington RM, et al. Virus-mediated EpoR76E Therapy Slows Optic Nerve Axonopathy in Experimental Glaucoma. Molecular therapy : the journal of the American Society of Gene Therapy. 2016;24(2):230-9.
56. Maddineni P, Kasetti RB, Patel PD, Millar JC, Kiehlbauch C, Clark AF, et al. CNS axonal degeneration and transport deficits at the optic nerve head precede structural and functional loss of retinal ganglion cells in a mouse model of glaucoma. MOL NEURODEGENER. 2020;15(1):48.
57. Wang X, Li Q, Liu C, Hall PA, Jiang J, Katchis CD, et al. Lin28 Signaling Supports Mammalian PNS and CNS Axon Regeneration. CELL REP. 2018;24(10):2540-52.
58. Berry M, Ahmed Z, Morgan-Warren P, Fulton D, Logan A. Prospects for mTOR-mediated functional repair after central nervous system trauma. NEUROBIOL DIS. 2016;85:99-110.

59. Puttagunta R, Tedeschi A, Sória MG, Hervera A, Lindner R, Rathore KI, et al. PCAF-dependent epigenetic changes promote axonal regeneration in the central nervous system. NAT COMMUN. 2014;5:3527.
60. Zhou B, Yu P, Lin M, Sun T, Chen Y, Sheng Z. Facilitation of axon regeneration by enhancing mitochondrial transport and rescuing energy deficits. The Journal of cell biology. 2016;214(1):103-19.
61. Xiong X, Wang X, Ewanek R, Bhat P, Diantonio A, Collins CA. Protein turnover of the Wallenda/DLK kinase regulates a retrograde response to axonal injury. The Journal of cell biology. 2010;191(1):211-23.
62. Eva R, Crisp S, Marland JRK, Norman JC, Kanamarlapudi V, ffrench-Constant C, et al. ARF6 directs axon transport and traffic of integrins and regulates axon growth in adult DRG neurons. The Journal of neuroscience : the official journal of the Society for Neuroscience. 2012;32(30):10352-64.
63. Pita-Thomas W, Mahar M, Joshi A, Gan D, Cavalli V. HDAC5 promotes optic nerve regeneration by activating the mTOR pathway. EXP NEUROL. 2019;317:271-83.
64. Li S, Yang C, Zhang L, Gao X, Wang X, Liu W, et al. Promoting axon regeneration in the adult CNS by modulation of the melanopsin/GPCR signaling. P NATL ACAD SCI USA. 2016;113(7):1937-42.
65. Duan X, Qiao M, Bei F, Kim I, He Z, Sanes JR. Subtype-specific regeneration of retinal ganglion cells following axotomy: effects of osteopontin and mTOR signaling. NEURON. 2015;85(6):1244-56.
66. Wang B, Jie Z, Joo D, Ordureau A, Liu P, Gan W, et al. TRAF2 and OTUD7B govern a ubiquitin-dependent switch that regulates mTORC2 signalling. NATURE. 2017;545(7654):365-9.
67. Tonoli H, Barrett JC. CD82 metastasis suppressor gene: a potential target for new therapeutics? TRENDS MOL MED. 2005;11(12):563-70.
68. Florin L, Lang T. Tetraspanin Assemblies in Virus Infection. FRONT IMMUNOL. 2018;9:1140.
69. Noy PJ, Yang J, Reyat JS, Matthews AL, Charlton AE, Furmston J, et al. TspanC8 Tetraspanins and A Disintegrin and Metalloprotease 10 (ADAM10) Interact via Their Extracellular Regions: EVIDENCE FOR DISTINCT BINDING MECHANISMS FOR DIFFERENT TspanC8 PROTEINS.; 2016. p. 3145-57.
70. Seipold L, Altmeppen H, Koudelka T, Tholey A, Kasparek P, Sedlacek R, et al. In vivo regulation of the A disintegrin and metalloproteinase 10 (ADAM10) by the tetraspanin 15. Cellular and molecular life sciences : CMLS. 2018;75(17):3251-67.
71. Yaseen IH, Monk PN, Partridge LJ. Tspan2: a tetraspanin protein involved in oligodendrogenesis and cancer metastasis. BIOCHEM SOC T. 2017;45(2):465-75.
72. Murru L, Moretto E, Martano G, Passafaro M. Tetraspanins shape the synapse. Molecular and cellular neurosciences. 2018;91:76-81.
73. Stuck MW, Conley SM, Naash MI. PRPH2/RDS and ROM-1: Historical context, current views and future considerations.; 2016. p. 47-63.

Figures

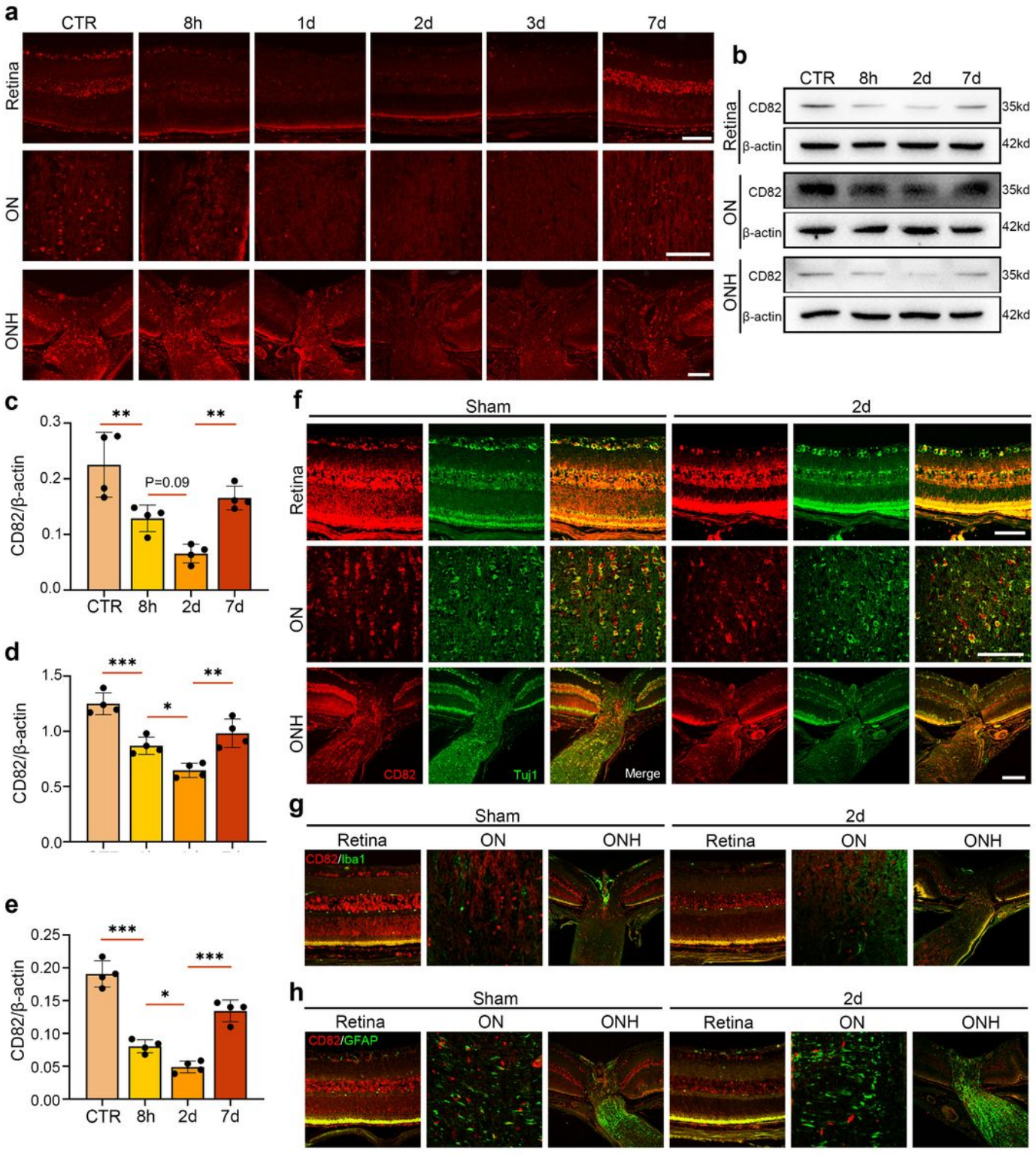

Figure 1

CD82 expression was down-regulated in retina, ONH and ON in the early stage after acute IOP hypertension. (a) Immunostaining of CD82 in mouse retina, ON, ONH at 8h, 1d, 2d, 3d, 7d after inducing AOHT, n=5 eyes for each group. Scale bar, 50μm. (b) Western blot showing protein levels of CD82 in mouse retina, ON and ONH tissues at 8h, 2d, 7d after AOHT. (c-e) Statistical analysis of the data shown in (b) from retina (c), ON (d) and ONH (e). The data were expressed as mean ± S.E.M., n=4, one-way ANOVA

*P<0.05, **P<0.01, ***P<0.001. (f-h) Co-immunofluorescent staining of CD82 (red) with RGC marker Tuj1 (green) (f), microglia marker Iba1 (green) (g), astrocyte marker (GFAP) (h) in mouse retina, ON, ONH in sham and 2d post-AOHT groups, n=4 eyes for each group. Scale bars, 50μm.

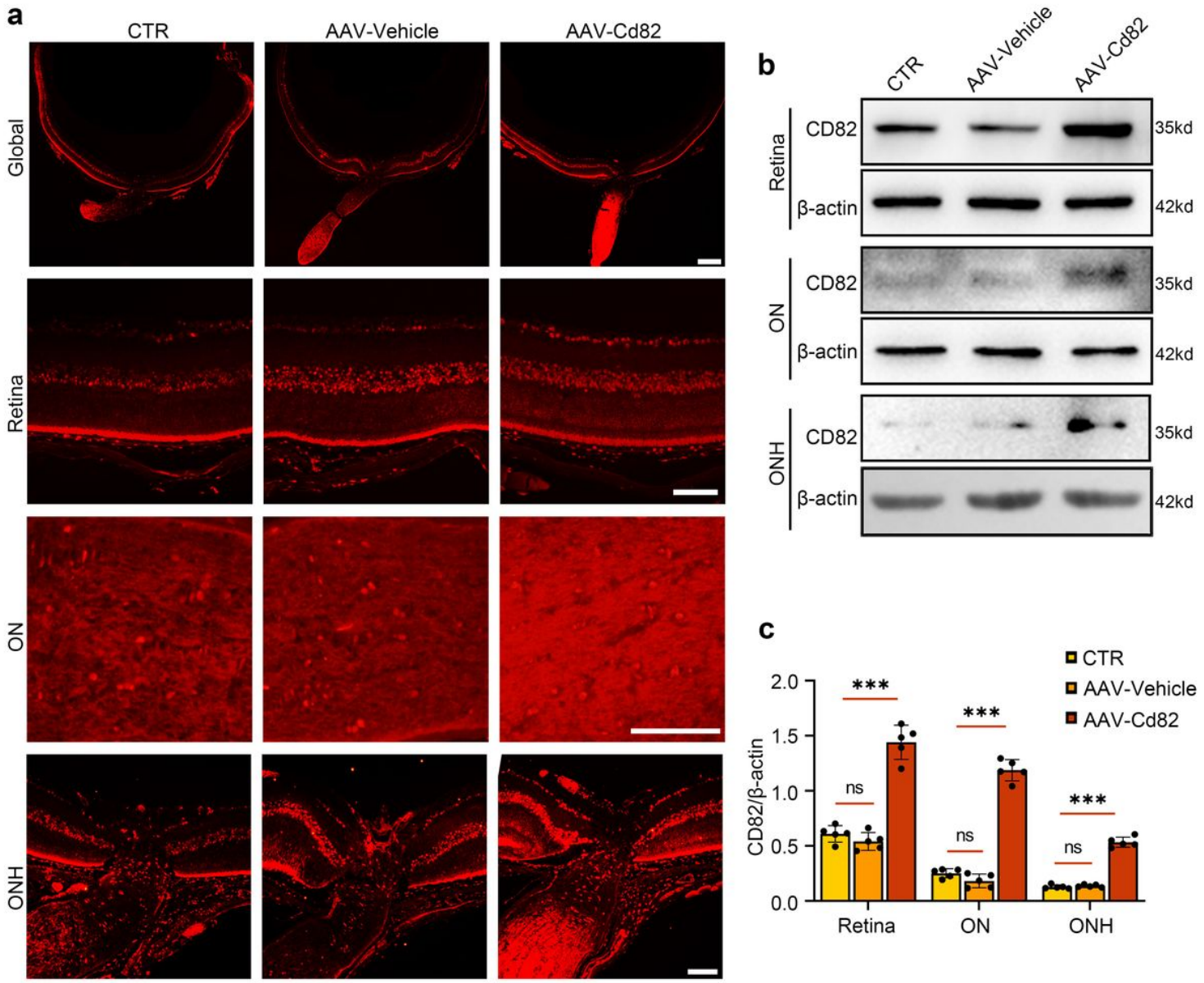

Figure 2

CD82 overexpression in retina and ON was achieved by Intravitreal injection of recombinant adeno-associated virus rAAV2/9-Cd82-mCherry. (a) Immunostaining of CD82 shown in whole globe, retina, ON and ONH in CTR, AAV-Vehicle, AAV-Cd82 groups 28 days after virus injection, n=5 eyes. Scale bars, 200μm for Global; 50μm for Retina, ON and ONH. (b) Western blot showing protein levels of CD82 in mouse retina, ON and ONH tissues from CTR, AAV-Vehicle, AAV-Cd82 groups 28 days after virus injection. (c) Statistical analysis of the data shown in (b). The data were expressed as mean ± S.E.M., n=5, one-way ANOVA ***P<0.001.

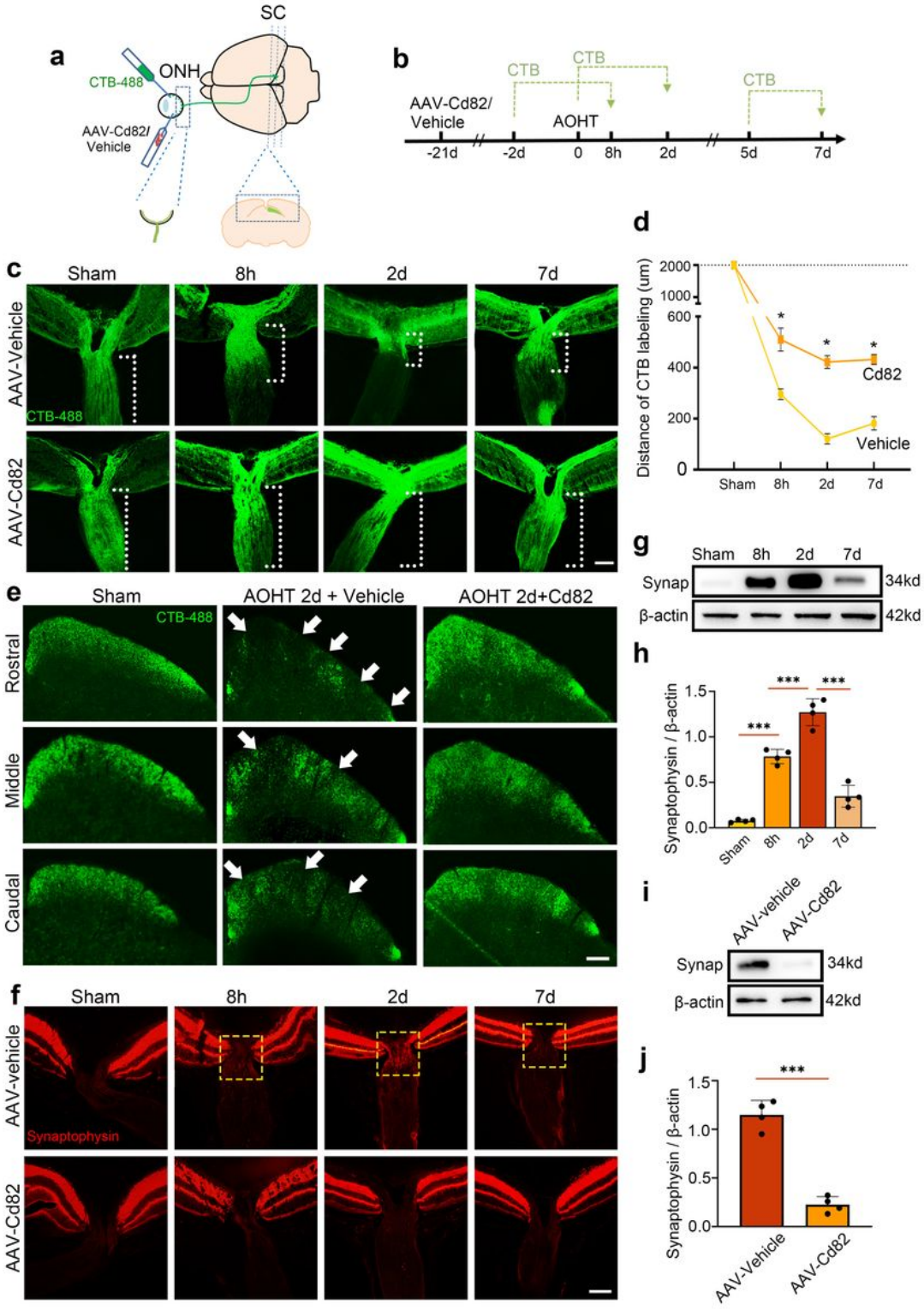

Figure 3

CD82 overexpression protected against axonal transport deficits after acute ocular hypertension. (a) Schematic drawing of AAV injection and CTB tracing from retina to SC. Dashed box indicating the observation site of ONH and SC. (b) Timeline of the major procedures for studying optic nerve transport. (c) Representative images showing anterogradely transported CTB-488 in ONH and proximal ON in groups of Sham, 8h, 2d and 7d post-AOHT with intravitreal injection of AAV-vehicle or AA-Cd82 obtained

at low exposure time of fluorescence microscopy. The white dashed lines indicating the distance of CTB labeling. Scale bar, 50μm. (d) Statistical analysis of the CTB labeling distance indicated in (c). The data were expressed as mean ± S.E.M., n=5 eyes, Student's t test for Cd82 v.s. vehicle at each time point, *p<0.05. (e) Representative images showing CTB-488 transported to SC from three layers as Rostral, Middle, and Caudal in groups of Sham and 2d post-AOHT with intravitreal injection of AAV-vehicle or AA-Cd82 obtained at high exposure time of fluorescence microscopy. The white arrow indicating defects of CTB distribution, n=5 mice. Scale bar, 200μm. (f) Immunostaining of Synaptophysin within ONH in the same groups as in (c). The yellow dashed box indicating accumulation of synaptophysin protein in ONH, n=5 eyes. Scale bar, 50μm. (g) Western blot showing protein levels of Synaptophysin in ONH tissues in groups of Sham, 8h, 2d and 7d post-AOHT. (h) Statistical analysis of the data shown in (g), n=4 eyes, one-way ANOVA, ***P<0.001. (i) Western blot showing protein levels of Synaptophysin in ONH tissues in groups of 2d-post AOHT with injection of AAV-vehicle or AA-Cd82. (j) Statistical analysis of the data shown in (i). The data were expressed as mean ± S.E.M., n=4 eyes, one-way ANOVA, ***P<0.001.

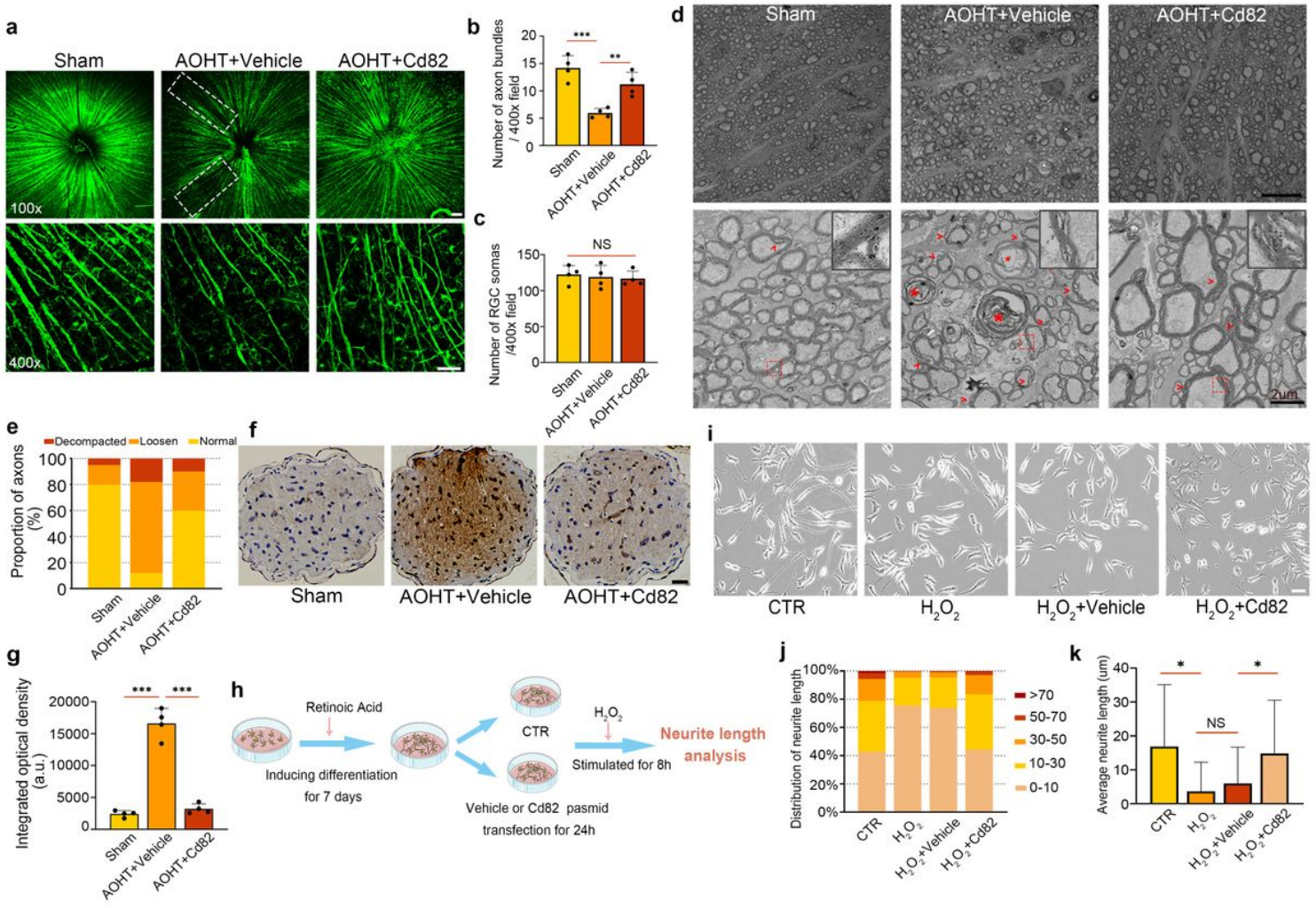

Figure 4

CD82 overexpression protected optic nerve from axonal degeneration induced by AOHT. (a) Immunostaining of Tuj1 in retina flat mount to show RGC axons in groups of Sham and 2d post-AOHT with or without CD82 overexpression. Top panel for images of 100x, scale bar, 100μm; Bottom panel for

images of 400x, scale bar, 50μm. The white dashed box indicating sparse axon distribution. (b&c) Statistical analysis of Tuj1+ axon bundles (b) and Tuj1+ RGCs (c) shown in the bottom panel of (a). The data were expressed as mean ± S.E.M., five nonoverlapping images was chosen for statistical analysis of each retina, n=4 retinas. (d) Electron microscopy images from optic nerve cross-section showing axon damage in groups of CTR and 2d post-AOHT with or without CD82 overexpression. Top panel, scale bar, 10μm; Bottom panel, scale bar, 2μm. Red arrowheads denoting delaminated myeline. Red asterisks representing spiral degeneration of axons. Right upper corner in each picture showing magnification of myelin sheath in red dashed boxes. (e) Statistical analysis of axon proportions with normal, loosen, or decompacted myelin as shown in (d). Five nonoverlapping images was chosen for statistical analysis of each individual, n=3 optic nerves. (f) Immunohistochemical staining of Aβ in optic nerve cross-section grouped as in (a). Scale bar, 20μm. (g) Statistical analysis of integrated optical density shown in (f), n=4 optic nerves. (h) Schematic drawing of the major procedures in neurite outgrowth analysis. (i) Representative images showing neurite outgrowth of SH-SY5Y cells in control group and H2O2 groups with or without Cd82 plasmid transfection. Scale bar, 20μm. (j & k) Statistical analysis of neurite length shown in (i). Twenty nonoverlapping fields of view chosen for analysis in each group for one experiment, n=400cells.Statistical tests in (b), (c), (g) and (k) using one-way ANOVA, *P<0.05, **P<0.01, ***P<0.001.

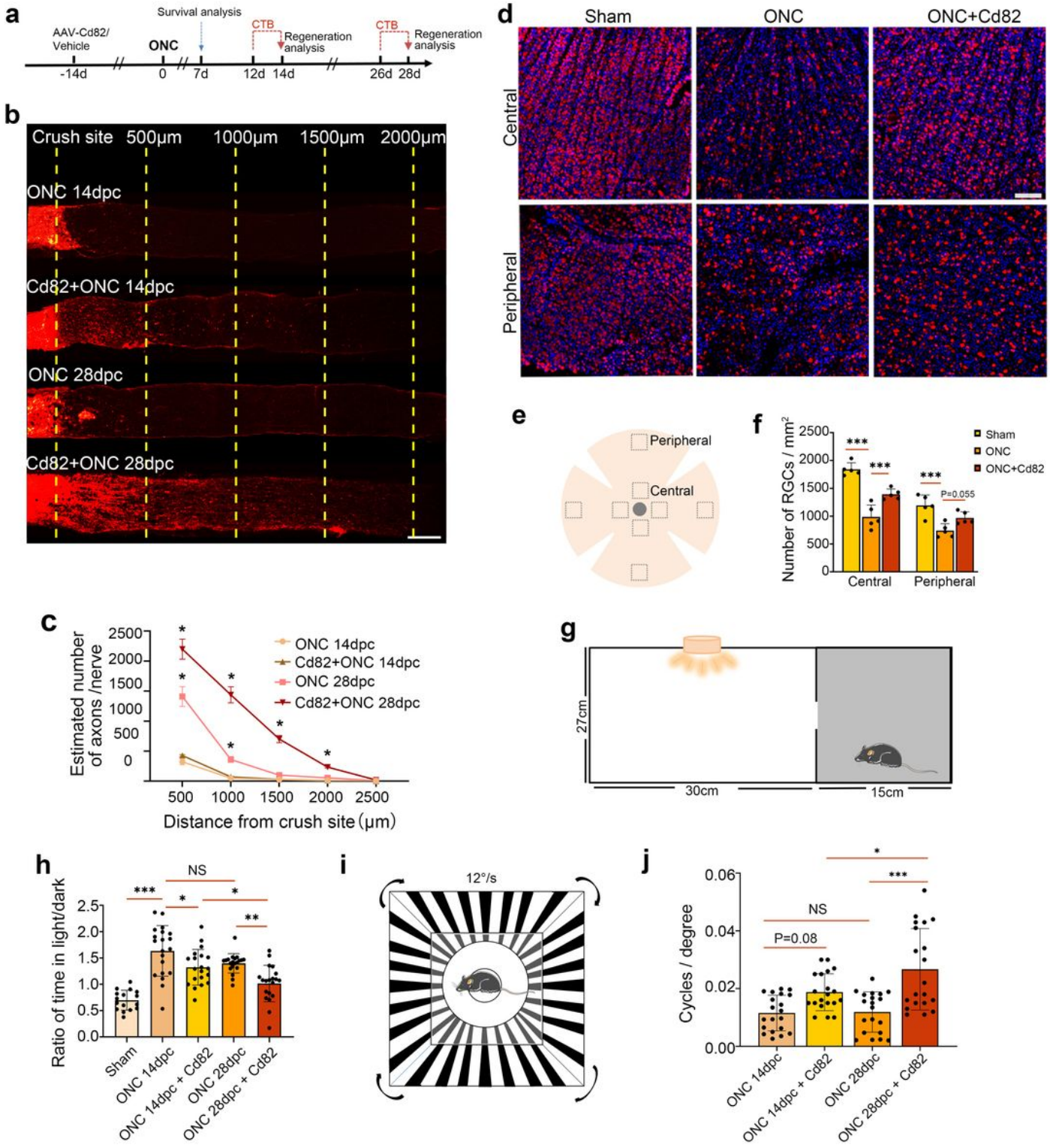

Figure 5

CD82 overexpression promoted axon regeneration, RGC survival, and visual function after optic nerve crush. (a) Timeline of the major procedures for exploring optic nerve regeneration and RGC survival after ONC. (b) Representative images showing axonal regeneration of optic nerve 14 or 28 days after ONC with or without CD82 overexpression. The yellow dashed line indicating the distances from the crush site. Scale bar, 200μm. (dpc=day post crush). (c) Statistical analysis of regenerated axons shown in (b), n=4

optic nerves, one-way ANOVA, p<0.05 for CD82+ONC 14dpc v.s ONC 14dpc and CD82+ONC 28dpc v.s ONC 28dpc. (d) Immunostaining of Rbpms in retina flat mount to mark RGC somas in control group and 7 day-post-ONC groups with or without CD82 overexpression. Scale bar, 100μm. (e) Schematic indicating observation area in retina flat mount. (f) Quantification of RGC numbers shown in (d). Four nonoverlapping fields of view chosen for analysis in each retina, n=4 retinas, one-way ANOVA, ***P<0.001. (g) Schematic drawing of mouse dark/light preference tests to evaluate light perception. (h) Statistical analysis of mouse dark/light preference tests. (i) Schematic drawing of mouse optomotor response tests to evaluate visual acuity. (j) Statistical analysis of mouse optomotor response. Statistical tests in (h) and (j) using one-way ANOVA, n=20 mice, *P<0.05, **P<0.01, ***P<0.001.

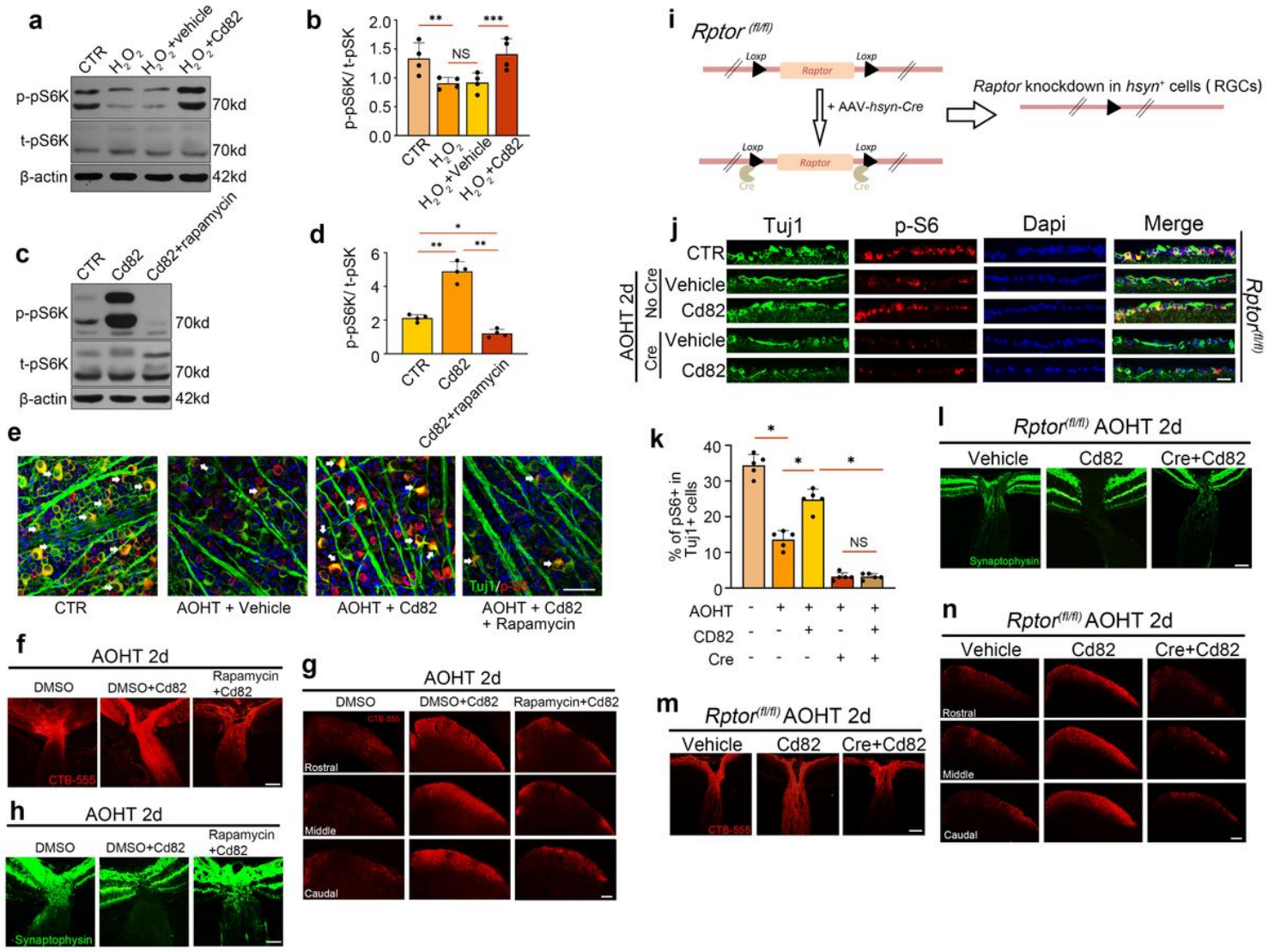

Figure 6

CD82 overexpression protected against axonal transport deficits through a mTORC1-dependent mechanism. (a) Western blot analysis of phosphorylated-pS6K and total pS6K in HEK-293T cells in CTR group and H2O2 groups with or without Cd82 plasmid transfection. (b) Statistical analysis of the data shown in (a), n=4. (c) Western blot analysis of phosphorylated pS6K and total pS6K in HEK-293T cells in CTR group and Cd82 plasmid transfected groups with or without Rapamycin. (d) Statistical analysis of

the data shown in (c), n=4. (e) Co-immunofluorescent staining of p-S6 (red) with RGC marker Tuj1 (green) in retina flat mount. Scale bar, 50μm. (f) Representative images showing anterogradely transported CTB-555 in ONH and proximal ON in Cd82 overexpression groups with or without rapamycin 2d after AOHT, n=5 eyes. Scale bar, 100μm. (g) Representative images showing CTB-555 transported to SC from three layers as Rostral, Middle, and Caudal, n=5 mice. Scale bar, 200μm. (h) Immunostaining of Synaptophysin within ONH, n=5 eyes. Scale bar, 100μm. (i) Schematic drawing of Cre induced conditional knockdown of Raptor in RGCs in Rptorfl/fl mouse. (j) Co-immunofluorescent staining of p-S6 (red) with RGC marker Tuj1 (green) in ganglion cell layer (GCL) of retina sections in vehicle or Cd82 overexpression groups with or without knockdown of Raptor by Cre. Scale bar, 50μm.¬ (k) Statistical analysis of p-S6 and Tuj1 co-labeling in GCL shown in (j), n=5 eyes. (l) Immunostaining of Synaptophysin within ONH in Cd82 overexpression groups with or without knockdown of Raptor 2d after AOHT, n=5 eyes. Scale bar, 100μm. (m) Representative images showing anterogradely transported CTB-555 in ONH and proximal ON, n=5 eyes. Scale bar, 100μm. (n) Representative images showing CTB-555 transported to SC from three layers as Rostral, Middle, and Caudal, n=5 mice. Scale bar, 200μm. Statistical tests in (b), (d) and (k) using one-way ANOVA, *P<0.05, **P<0.01, ***P<0.001.

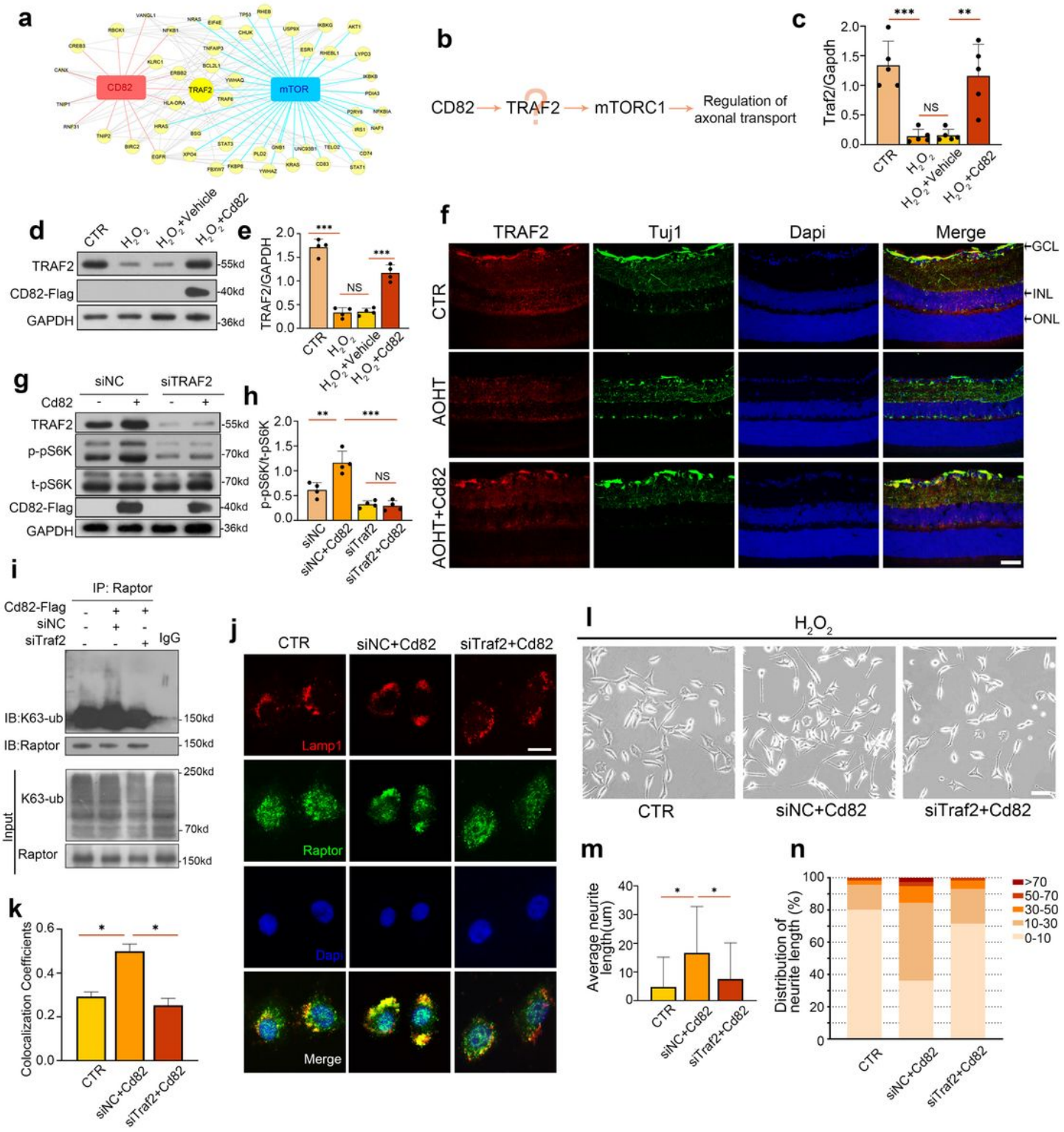

Figure 7

CD82 activated mTORC1 via TRAF2 mediated k63-linked ubiquitylation to protect against neurodegeneration. (a) PPI network of hub molecules connecting CD82 with mTOR. Node size reflected the compositive correlation with CD82 and mTOR. (b) The putative pathway of TRAF2 mediated activation of mTORC1 downstream of CD82. (c) RT-PCR analysis of Traf2 mRNA in HEK-293T cells in CTR group and H2O2 groups with or without Cd82 plasmid transfection, n=5. (d) Western blot analysis of

TRAF2 protein level in HEK-293T cells in CTR group and H2O2 groups with or without Cd82 plasmid transfection. (e) Statistical analysis of the data shown in (d), n=4. (f) Immunostaining of TRAF2 (red) with RGC marker Tuj1 (green) in retina sections of control group and 2d post-AOHT groups with or without AAV-Cd82, n=5 retinas. Scale bar, 50μm. GCL= ganglion cell layer, INL= inner nuclear layer, ONL= outer nuclear layer. (g) Western blot analysis of phosphorylated pS6K and total pS6K in HEK-293T cells in siNC group or siTraf2 group with or without Cd82 plasmid transfection. (h) Statistical analysis of the data shown in (g), n=4. (i) Immunoprecipitation of K63-linked ubiquitination with raptor in control group and Cd82 overexpression groups with or without siTraf2, n=3. (j) Co-immunofluorescent staining of Raptor (green) with the lysosome marker Lamp1 (red) in SH-SY5Y cells of control group and Cd82 overexpression groups with or without siTraf2. Scale bar, 20μm. (k) Statistical analysis of Raptor and Lamp1 colocalization in SH-SY5Y cells shown in (j), n=50 cells. (l) Representative images showing neurite outgrowth of SH-SY5Y cells in the same group as in (j). Scale bar, 20μm. (m&n) Statistical analysis of neurite length shown in (l), n=100 cells. Statistical tests in (c), (e), (h), (k) and (m) using one-way ANOVA, *P<0.05, **P<0.01, ***P<0.001.

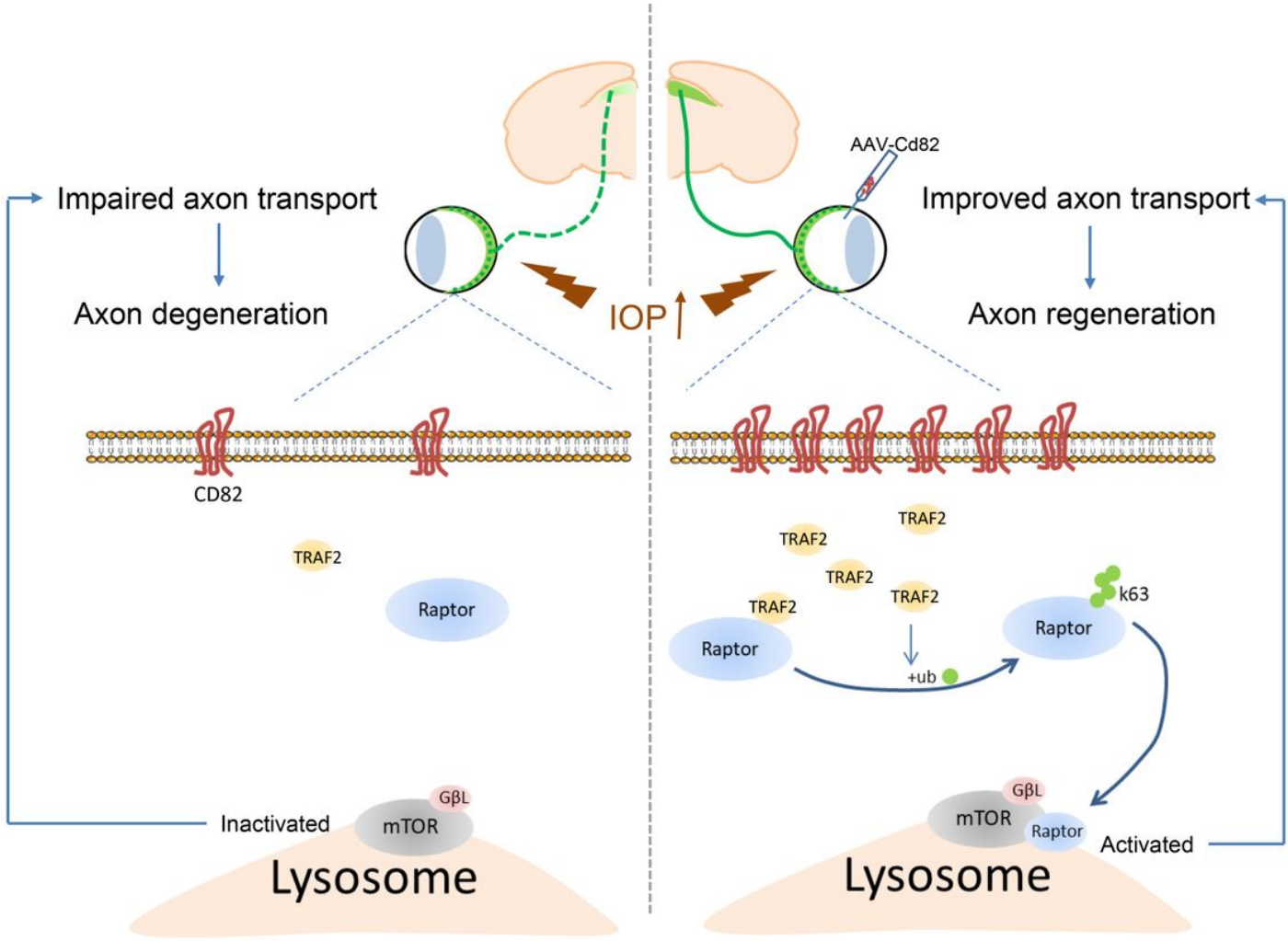

Figure 8

Schematic representation of CD82 neuroprotection effect after ocular hypertension. Acute ocular hypertension induced axonal transport deficits and subsequently caused axon degeneration. CD82 overexpression protected against axon injury through upregulating TRAF2, which activates mTORC1 through K63-linked ubiquitylation and intracellular repositioning of Raptor.

Supplementary Files

This is a list of supplementary files associated with this preprint. Click to download.

- FigureS1.tif
- FigureS2.tif